Payoff selectivity unlocks collective intelligence in naturalistic human groups

Valerii Chirkov[1,2,3*], Ralf H.J.M. Kurvers[1,2], Pawel Romanczuk[2,3] & Dominik Deffner[1,2,4*]

[1]Center for Adaptive Rationality, Max Planck Institute for Human Development, Berlin, Germany
[2]Science of Intelligence Excellence Cluster, Technical University Berlin, Berlin, Germany
[3]Institute for Theoretical Biology, Humboldt University Berlin, Berlin, Germany
[4]Department of Psychology, Marburg University, Marburg, Germany
*Corresponding authors: valerii.chirkov@hu-berlin.de; dominik.deffner@uni-marburg.de

Humans' abilities for complex social learning and collective adaptation are unparalleled across species. Yet it is largely unknown how people integrate dynamically changing personal and social cues in realistic environments, resulting in collective intelligence or maladaptive behavior. Here, we report an online 3D immersive-reality experiment in which participants ($n = 621$) searched for and tracked a mobile resource under realistic visual–spatial constraints. Participants completed the task either alone or in groups of five with different types of social information and resource speeds. Contrasting earlier work, participants in groups outperformed solitary individuals, but only when payoff information was available. High-resolution visual field data and movement trajectories revealed that payoff visibility prompted adaptive recalibration of visual information flow, thereby enabling flexible adaptation. Computational models of fine-grained movement decisions and agent-based simulations showed that payoff information let participants dynamically identify and selectively respond to reliable social cues, thus unlocking the group's collective potential.

Humans are uniquely flexible decision-makers, dynamically combining personal and social sources of information (Laland, 2004; Deffner et al., 2020; Tump et al., 2020; Wu et al., 2025). Social information can inform adaptive behavior and facilitate collective adaptation to fluctuating environments (Henrich & McElreath, 2003; Galesic et al., 2023), but not all social information is equally useful, and overreliance on others can result in maladaptive herding and collective breakdown (Toyokawa et al., 2019; Tump et al., 2020; Deffner et al., 2024). Moving beyond cataloging social learning strategies (Laland, 2004; Kendal et al., 2018a), recent studies have investigated the flexible integration of different social and asocial cues, linking individual-level strategies to collective adaptations (Toyokawa et al., 2019; Deffner et al., 2024; Wu et al., 2025). Emerging theoretical frameworks suggest that the same cognitive mechanisms might underlie learning about both social and non-social environmental features, with individuals assessing social cues as indicators of potential rewards (Heyes, 2016; Schultner et al., 2025).

The cues individuals rely on in realistic collective scenarios and how they arbitrate between dynamically changing social and non-social features to achieve collective intelligence remains poorly understood. Most previous experiments relied on simplified paradigms in which participants chose from a limited set of options at fixed intervals and social information was presented in a structured and summarized format (Tump et al., 2024). Such paradigms lack the visual–spatial richness of real-world social dynamics, where perceptual and spatial constraints fundamentally shape the costs and benefits of social information use (Mezey et al., 2024; Wu et al., 2025). These simplified paradigms typically assume that relevant social features are

predefined, instead of requiring participants to infer which features are reliably associated with success (Schultner et al., 2025). To understand the social-learning mechanisms governing adaptive and maladaptive outcomes in real-world collectives, paradigms that allow complex social dynamics to unfold within naturalistic environments are essential.

We used a large-scale immersive-reality approach to study how groups of online participants search for and track a mobile resource. Collective search provides an ideal testbed to study dynamic social learning and collective behavior in a controlled, yet ecologically relevant, context (Deffner et al., 2024; Garg et al., 2024; Mezey et al., 2024; Wu et al., 2025; Schakowski et al., 2025). Previous theoretical work and experiments with fish have uncovered the self-organized "collective sensing" phenomenon, where collectives successfully detect and track a rewarding location in the environment using rudimentary processing of personal information (Berdahl et al., 2013; Hein et al., 2015; Puckett et al., 2018). Instead of solving the complicated inference problem of tracking shifting environmental gradients, individuals can collectively adapt to complex environments by responding to simple social cues, such as the location of other animals. In a series of experiments mirroring the original work on fish, Hawkins et al. (2023) showed that without payoff information, human participants could infer the location of a hidden scoring region based on observable movement trajectories, suggesting powerful social inference. This paradigm, however, used an unrealistic bird's-eye view, representing participants as moving shapes on a flat surface. Participants could directly see when others stopped moving; while reliable, this type of cue for social inference is usually unavailable outside the lab. Moreover, people in the real world often need to balance personal and social information simultaneously. Monitoring one's own personal reward rates as well as the behavior of others might interfere with the adaptive calibration of social information use. To study collective search and tracking in a more realistic scenario with a limited first-person field of view, realistic spatial constraints, and continuous integration of personal and social information, we developed a 3D immersive-reality experiment that created a natural trade-off between individual exploration of the environment and social learning (Rahmani et al., 2020; Bastien & Romanczuk, 2020; Deffner et al., 2024; Wu et al., 2025).

Participants ($n = 621$) were instructed to search and track a hidden moving resource to maximize a monetary reward (Fig. 1; see "Methods" for details; Supplementary Video 1). The closer participants were to its center, the more points they collected. Participants could find and track the resource by looking at their avatar's detector values, indicating their current distance to the resource center (Fig. 1B; Supplementary Videos 2 and 3). Participants completed 15 min of the task in a 4×2 between-subjects design (Fig. 1C). Across four conditions, participants completed the task by themselves (*Alone*, A), in groups where they could see others but had no information about their payoffs (*No Payoff-Sharing*, NP), in groups where others' current payoffs were always indicated by a colored sign above their heads (*Full Payoff-Sharing*, FP), or in groups where participants could freely decide whether and when to share their current payoffs at a small cost (*Voluntary Payoff-Sharing*, VP). Participants experienced either a slow or fast resource, moving at 40% or 80% of their avatar's speed, respectively. The resource movement followed a Lévy walk consisting of frequent short steps and rare long steps, characteristic of biological movement across scales (Zaburdaev et al., 2015). Fig. 1D shows that the optimal rotation magnitude (i.e., the degree to which people turn relative to the previous movement direction) follows a simple heuristic: A rapid decrease in detector value (indicating moving

away from the resource center) should prompt large rotations, while a sharp increase in detector value (indicating moving toward the center) should prompt continued movement in the same direction. The ranges of optimal rotations are narrower for the slow resource because there is less uncertainty about the location of the resource center (see Supplementary Information Section S4 for the mathematical derivation of the optimal rotation model and Figs. 1D and S2 for illustration).

Based on the collective sensing literature, we predicted that search and tracking would be more efficient for collectives than for solitary individuals, resulting in better performance in the No Payoff-Sharing and Full Payoff-Sharing conditions compared to the Alone condition (see preregistration at AsPredicted: https://aspredicted.org/C62_M6Z). We further predicted that within our dynamically changing immersive environment, the location of others would be insufficient for full social inference, resulting in superior performance in the Full Payoff-Sharing condition compared to the No Payoff-Sharing condition. Finally, simulation work has shown that unconditional sharing of payoff information can evolve in collective search, acting as a recruitment signal that facilitates the self-organization of groups (Tump et al., 2019). We therefore predicted that participants in the Voluntary Payoff-Sharing condition would pay a small cost to share payoff information, and that their performance would fall in between the performance of participants in the No Payoff-Sharing and Full Payoff-Sharing conditions.

Our behavioral analyses (Fig. 2) show that sociality was a double-edged sword: Participants in groups could outperform solitary individuals through both superior tracking and search performance, but only when full payoff information was available; in the absence of payoff information, they sometimes even performed worse, especially when tracking a fast-moving resource. We leveraged high-resolution time-series data of participants' visual information and movement trajectories to study how key events (e.g., resource discoveries) triggered adaptive changes in visibility networks (Fig. 3). We found that payoff information boosted performance by allowing collectives to flexibly reorganize visibility networks over time and adaptively guide information flow between group members. We then designed a computational model predicting movement decisions on a second-to-second resolution to test how private and social features jointly guided participants' movement behavior (Fig. 4). Computational results confirmed that payoff information unlocked collective intelligence by allowing participants to selectively tune their responses to the position and movement direction of successful peers. Finally, to link our mechanistic insights back to the observed collective dynamics and to gain generalizable insights beyond the specific settings of our experiment, we developed an agent-based simulation, which corroborated our finding that payoff selectivity was indeed the key factor promoting adaptive collective outcomes—but only in certain types of environments (Fig. 5).

Results

Performance depends on the social environment and resource speed

We start by comparing performance across the eight treatment conditions to show that collective intelligence only arises under certain circumstances. We use three performance metrics: tracking time (i.e., proportion of time participants spent on the resource), tracking efficiency (i.e., average number of points collected when participants were on the resource), and total

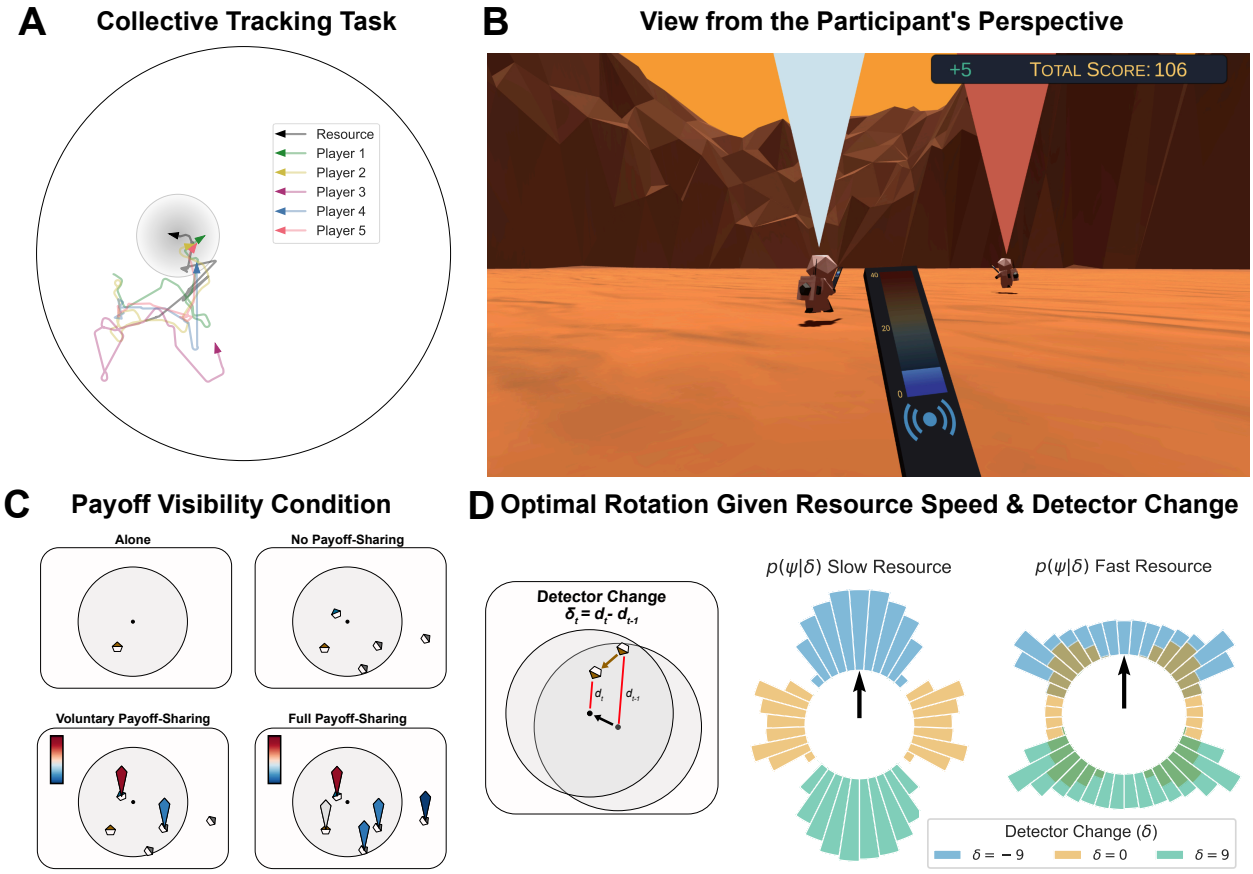

Figure 1: Collective tracking task. (A) Example trajectories of the resource (shaded gray disc) and five participants (colored lines) in a circular arena. Arrows indicate direction of movement. **(B)** Screen capture from the Voluntary Payoff-Sharing condition. Participants control virtual avatars from a first-person perspective and can move freely through the arena. Each avatar is equipped with a resource detector showing the rate of point collection (i.e., the proximity to the resource center); dark red (blue) indicates that the participant is close to (far from) the resource center. The number of points gained is also indicated in the top right corner of the screen. If available, other participants' current payoffs (i.e., their proximity to the resource center) is indicated by a colored beam above their avatar, following the same color scheme as for the detectors. Here, the participant on the right is closer to the resource center, providing high-quality social information. **(C)** Payoff visibility conditions. Alone: Participants are alone in the environment; No Payoff-Sharing: Participants are in groups of five and can observe others' positions, but not their current payoffs; Voluntary Payoff-Sharing: Participants are in groups of five and can continuously decide whether to share the payoff of their current location or not (at a small cost of 1 point per second); Full Payoff-Sharing: Participants are in groups of five and their payoff information is always shared (at no cost). **(D) Left**: Participants' private information consists of changes in their detector value (δ_t), which indicates the change in distance to the resource center at time t. **Middle** and **right**: Probabilities of optimal rotation (ψ) as a function of detector value change (δ) from the previous time step (in seconds), mathematically derived and numerically computed for slow and fast resource movement. While the exact optimal rotation angle cannot be inferred from δ, the optimal rotation magnitude follows a simple heuristic: ψ scales linearly with δ (see Supplementary Information Section S4 for the mathematical derivation of the optimal rotation model). This means that sharp increase in points call for minimal rotation, whereas sharp decrease call for maximal rotation.

number of points, which is a function of both components (color gradient in Fig. 2A). Using hierarchical Bayesian regressions (see Methods), we found that, unsurprisingly, participants in the slow resource environment collected more points than those in the fast resource environment (posterior contrast: 10,679.04 [9,789.29, 11,544.90]; Fig. 2A; see Figs. S3, S4, S5 for participant-level scores, tracking times, and tracking efficiencies).

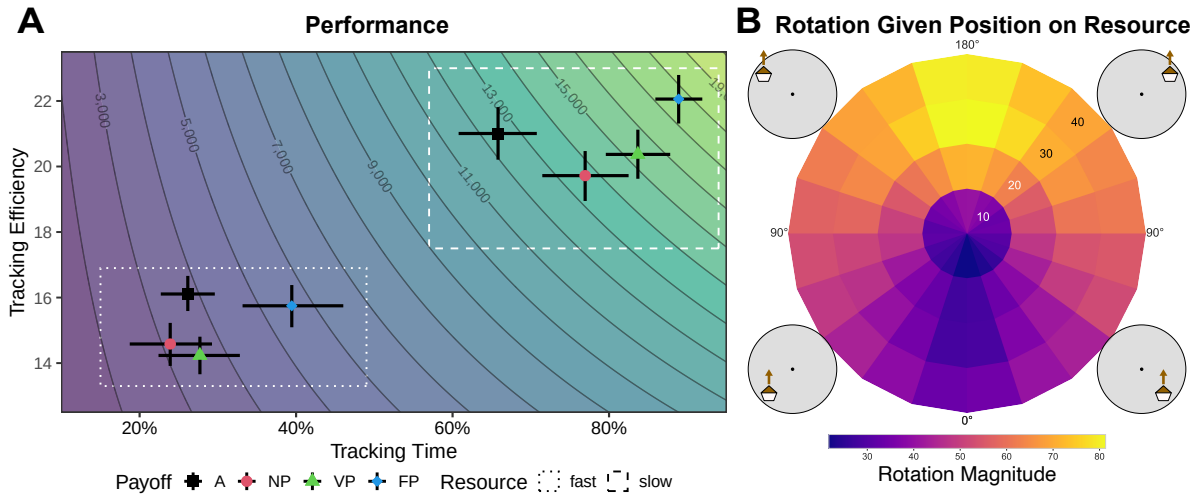

Figure 2: **(A)** Mean tracking time, tracking efficiency, and total score (colored isoclines) per treatment. A: Alone Condition; NP: No Payoff-Sharing; VP: Voluntary Payoff-Sharing; FP: Full Payoff-Sharing. Dots and error bars show posterior means and 90% HPDIs. **(B)** Participants' average rotation magnitude for different positions on the resource.

In the slow resource environment (dashed box in Fig. 2A), participants in all three group conditions collected more points compared to solitary participants (NP: 1,286.73 [−790.97, 3,366.14], VP: 3,137.53 [1,126.32, 5,079.08]; FP: 5,236.22 [3,373.83, 7,129.94]). Participants in groups with full payoff information (FP) collected more points than participants in groups with no payoff information (3,949.48 [1,876.26, 6,081.79]), with performance in the voluntary payoff condition (VP) falling in between (see Supplementary Information Section S5 for details on payoff sharing behavior). Groups outperformed singletons mainly because participants in groups spent more time on the resource (NP: 1.67 [0.56, 2.71]; VP: 2.68 [1.75, 3.63]; FP 3.47 [2.63, 4.32]). Only participants in the FP condition had higher tracking efficiency than singletons (1.05 [−0.02, 2.16]), whereas participants in the NP and VP conditions tended to perform worse than singletons (NP: −1.29 [−2.38, −0.16]; VP: −0.64 [−1.73, 0.46]).

In the fast resource environment (dotted box in Fig. 2A), only participants in FP groups collected more points than solitary ones (1,710.26 [572.81, 2,803.50]). Participants in VP groups performed on par with singletons (−298.66 [−1,169.61, 537.86]), and participants in NP groups performed worse than singletons (−834.66 [−1,654.19, −35.59]). The superior performance of participants in FP groups resulted from them spending more time on the resource while achieving equal tracking efficiency compared to singletons. Participants in NP and VP groups, on the other hand, had similar tracking times but substantially worse tracking efficiency than singletons, resulting in worse overall performance (see Tables S2, S4, and S5 for statistical comparisons of scores, tracking times, and tracking efficiencies). Participants in the FP condition had the lowest variability in points collected in both resource environments, whereas single participants had the highest (Table S3), suggesting that collective foraging can buffer the risks of searching for resources in dynamic environments (Caraco, 1981). In sum, these results suggest that in slow-changing environments, it is beneficial to be in a group. In fast-changing environments, however, merely observing the location of others may lead to maladaptive use of social information, which can only be offset by additional payoff information.

Our mathematical derivation (Fig. 1D; Supplementary Information Section S4) revealed a

simple heuristic for optimal rotation for tracking the resource: Rotate if the detector value decreases, and continue in the same direction if it increases. Across conditions, participants followed this heuristic (Fig. 2B; see Fig. S6 for condition-specific results). When they were moving towards the center of the resource, they displayed a relatively small angle of rotation; when they were moving away from the center, they displayed a large angle of rotation.

Payoff information shapes the structure and adaptability of visibility networks

We used visibility network analysis to show that payoff information increased adaptive visual connectivity and boosted performance by allowing collectives to flexibly reorganize visibility networks over time. At both resource speeds, participants in FP groups had higher overall connectivity, with both higher in- and out-degrees, than did participants in NP and VP groups (Fig. 3A; see Tables S6 and S7 for statical comparisons). This suggests that participants looked more at others when information about others' payoffs was available. In all conditions, we observed a strong negative correlation between participants' in- and out-degrees (Fig. S8), replicating previous results from an immersive foraging experiment with static rewards (Wu et al., 2025). This suggests an asymmetry in the flow of social information, with some participants being frequently observed by others while rarely observing others themselves, and other participants frequently observing others while rarely being observed themselves. Participants' in-degree and out-degree were systematically related to their performance in almost all conditions (Fig. S9). Participants who collected more points paid little visual attention to others (low out-degree), but received a lot of visual attention from others (high in-degree). High-performing participants became focal points. These effects were strongest in the FP conditions, and weakest in the NP conditions, suggesting that the availability of high-quality social information provided more scope for adaptive selective visual attention.

We next quantified the differences in quality of social information across conditions. To capture the potential for beneficial social information use, for all times when participants had one or more other participants in their field of view, we calculated the probability that at least one of these other participants was closer to the resource center than the focal participant. Across resource speeds, and when both searching and tracking, participants in the FP groups were more likely to observe others in better positions than themselves compared to participants in the NP and VP groups (fast/searching: NP 0.20 [0.18, 0.23], VP 0.13 [0.11, 0.15]; slow/searching: NP 0.12 [0.10, 0.15], VP 0.08 [0.06, 0.11]; fast/tracking: NP 0.14 [0.12, 0.16], VP 0.10 [0.08, 0.12]; slow/tracking: NP 0.05 [0.03, 0.06], VP 0.02 [0.01, 0.04]; Fig. 3B; see Table S8 for statistical comparisons). In sum, payoff information increased overall social connectivity (Fig. 3A), as well as the adaptiveness of social connectivity (Fig. 3B).

We studied the temporal adaptation of visibility networks by analyzing how participants changed their visual attention in situations where one participant discovered the resource while the others were searching for it (Fig. 3C; see Methods for details). The frequency of such events was much higher in the fast resource environment (829 instances for fast vs. 261 for slow; see Table S9), since participants were more likely to lose (and rediscover) the resource when it moved quickly. We therefore focus on the fast resource environments in the main text (see Fig. S11 for results for the slow environments). In the FP condition, participants who

discovered the resource (the "discoverer") received much more visual attention (i.e., in-degree) shortly after discovery—peaking approximately 10 s after discovery—compared to discoverers in NP and VP groups (NP: 0.80 [0.72, 0.88]; VP: 0.62 [0.54, 0.70]; Fig. 3C, bottom left). The other participants ("others") increased their visual attention to others (i.e., out-degree) after the resource discovery. Comparing the in-degree of discoverers and others shows that others oriented specifically toward the discoverer (see Figs. S12, S13). Again, this effect was much stronger for participants in the FP groups compared to participants in the NP and VP groups (NP: 0.32 [0.29, 0.36]; VP: 0.27 [0.23, 0.30]; Fig. 3C, bottom right). Notably, the VP condition also revealed distinct outcomes depending on whether the discoverer shared their payoff or not, replicating between-condition differences: Discoverers who shared their payoffs received more visual attention and others increased their outward attention (see Fig. S14 for fast resources and Fig. S15 for slow resources), suggesting that payoff sharing triggered adaptive network responses.

This reconfiguration of visibility networks after resource discoveries had tangible adaptive consequences. The probability that "others" would be on the resource increased more markedly over time in the FP condition compared to the other conditions (Fig. 3C, top right). Moreover, this greater availability of local social information allowed discoverers in FP groups to stay on the resource for longer compared to solitary individuals who discovered the resource, whereas discoverers in other group conditions lost it sooner (Fig. 3C, top left; see Figs. S14, S15 for corroborating results comparing sharing and non-sharing events in the VP condition). These results underscore how continued access to payoff information enabled FP groups to quickly adapt their visibility networks over time and achieve a higher tracking time than participants in NP and VP groups (Fig. 2A). Others were able to capitalize on the discoveries of group members, and even discoverers themselves benefited from the recruitment of social information to their local environment.

Computational model of movement decisions

To show how behavioral outcomes arose from participants' fine-grained decisions, we developed a computational model of movement decisions that formalizes hypotheses about the relative importance participants place on different private and social cues (Fig. 4). We modeled participants' absolute changes in movement direction as a linear combination of private and social features. We used the magnitude of rotations instead of directions because our mathematical derivations showed that changes in detector values only provide information on how much an optimal agent should rotate, and not in which direction (see Supplementary Information Section S6 and Figs. S16, S17 for an analysis of rotation direction that reaches the same main conclusions). Search and tracking were analyzed in separate models because different sets of features were available for each state.

Private information features

To study how participants responded to their personal rewards, we quantified two features: The *distance* feature reflects a participant's distance to the resource center, which they can infer from their absolute detector value, and the *detector change* feature reflects the change in this distance since the previous time step (in seconds), which is the key factor determining optimal

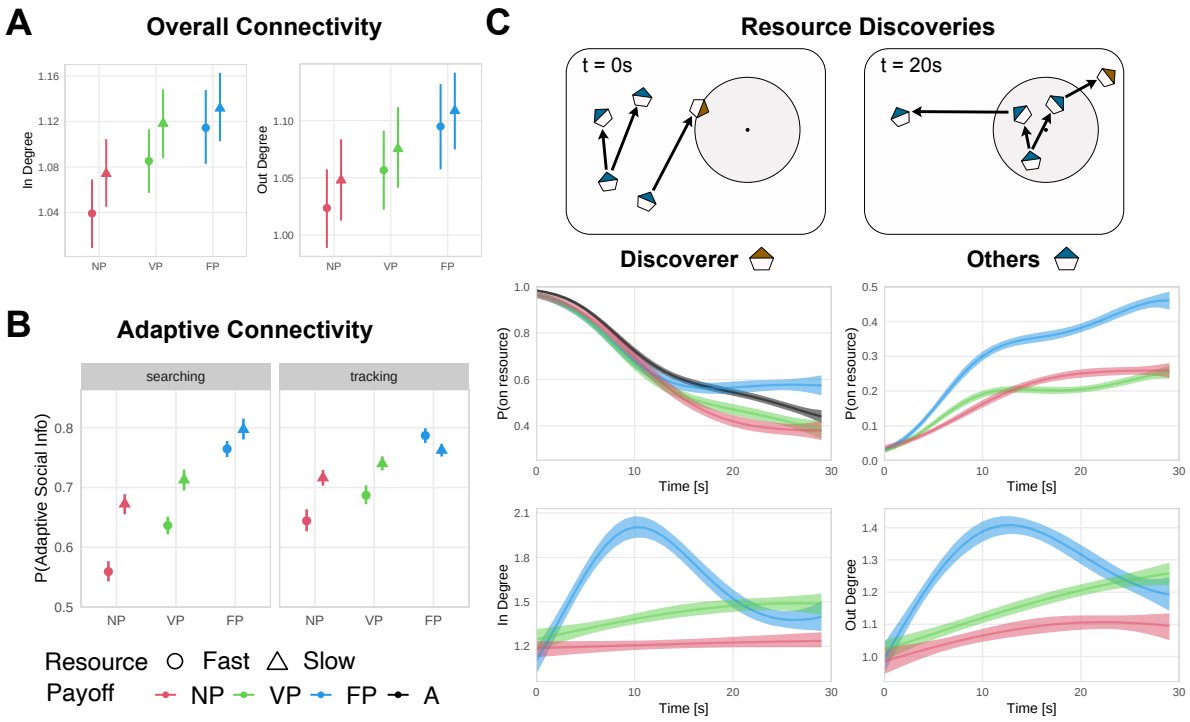

Figure 3: Visibility network analysis. (A) Average in-degree and out-degree per payoff-sharing condition. **(B)** Probability for participants who have one or more other participants in their field of view that at least one of these others is closer to the resource center than they are (adaptive social information), per payoff-sharing condition and for searching and tracking. **(C) Top**: Illustration of a resource discovery event, where a "discoverer" (brown) enters the resource and the "others" (blue) shift their visual attention (indicated by arrows) to the discoverer and approach the resource center 20 s later. **Middle left**: Probability of remaining on the resource for the initial discoverer, conditional on time since the discovery event. **Middle right**: Probability that the others (i.e., non-discoverers) are on the resource, conditional on time since discovery. **Bottom left**: Average in-degree of the discoverer over time. **Bottom right**: Average out-degree of others over time. Black line indicates participants in the Alone condition. Dark lines show posterior means of a Bayesian Gaussian process regression; shades represent 90% HPDIs.

tracking according to our analytical derivation. Note that both features were only available to participants when they were on the resource.

Social information features

To study how participants responded to different visible social cues, we quantified four social features. The *position of others* represents the angular difference between a participant's heading direction and the average position of others within a participant's field of view, thus indicating where others are. The *movement direction of others* reflects the angular difference between a participant's heading direction and the average movement direction of others within their field of view, indicating where others are going. We also included the interactions between each of these features and *social information quality*. For tracking, social information quality is computed as the difference between one's own distance to the center and the average distance of visible others. For searching, the value of social information quality is set to 1 if another visible participant is currently on the resource and to -1 otherwise. These interactions allow for adaptive tuning of social information use depending on the performance of others (which may or may not be directly visible, depending on the condition). All features were normalized to a

range between $[-1, 1]$ to allow for comparisons of all shared features across conditions.

Model weights

When tracking the resource, participants in all conditions rotated more if they were further from the resource center and if their distance to the center had increased within the last second (i.e., their payoffs decreased; see Fig. 4B). Participants responded most strongly to detector changes in the alone condition; participants in the FP groups responded least strongly. This reduced reliance on private cues in the presence of increasingly reliable forms of social information confirms the attentional and/or behavioral trade-off between private and social cues and raises a key question: If optimal rotation during tracking is purely determined by the current change in payoffs and FP groups were least sensitive to this key piece of private information, how were they able to outperform all other conditions in slow environments and match singletons in fast environments?

The answer lies in their more selective use of social information. Overall, participants used social information to inform their movement choices (all social information feature weights greater than 0) and social information features influenced participants' rotation decisions similarly across both tracking and search states and across both resource speeds (Fig. 4C). However, there were crucial differences among payoff sharing conditions. Participants in all group conditions relied on the position of others: They rotated more if others were in the periphery of their field of view. Participants in FP groups tended to respond most strongly to others' positions (except when searching in the slow resource environment). Mirroring the behavioral results, the behavior of participants in VP groups tended to fall in between that of the FP and NP groups. Participants also relied on the movement direction of others, rotating more if their movement direction differed greatly from the average movement direction of others in their field of view. Once again, participants in the FP condition responded most strongly to the movement direction of others compared to NP and VP conditions, and the performance of participants in VP groups tended to fall in between that of the FP and NP groups.

Next, we turn to the interaction between the social features and social information quality in order to examine the selectivity in participants' reliance on social information. Participants in FP groups flexibly tuned their social information use, responding more strongly to the position and movement direction of others if they provided higher-quality information. In the slow resource environment, participants in NP groups, where payoff information was not explicitly shared, also adjusted their behavior based on the payoffs of others. This finding suggests that they were able to infer the success of others solely based on their behavior—albeit to a limited degree. In the fast resource environment, however, only participants with visible payoff information could flexibly adjust their reliance on the behavior of others, suggesting important limits to social inference in fast-changing environments. More generally, differences in use of social cues between payoff-sharing conditions were much more pronounced in fast resource environments (both during tracking and searching) than in slow resource environments.

To identify the adaptive consequences of decision-making, we used the random effects of the feature weights from the multilevel computational model to predict success in terms of tracking efficiency and tracking time (see Supplementary Information Section S7). Higher detector sensitivity was generally associated with higher tracking efficiency across all conditions.

Following others' positions was associated with lower tracking efficiency, whereas aligning with others' movement direction was associated with higher efficiency (see Fig. S18), suggesting that where others were going was a more reliable cue for success than where they were. Importantly, selectivity with respect to both position and movement direction of others was reliably associated with tracking efficiency, again confirming that selective tuning of social information use depending on payoffs was crucial for success (see Fig. S19 for results on searching that confirm the core insights).

In sum, the computational model highlights the critical role of social information quality in shaping participants' movement decisions. When payoff information was available, participants overall relied more on social cues. They modulated their social information use depending on information quality by selectively using social cues when others were performing better than themselves. The model also allowed us to examine how flexibly participants integrated social and private information features, revealing a dynamic trade-off based on contextual factors.

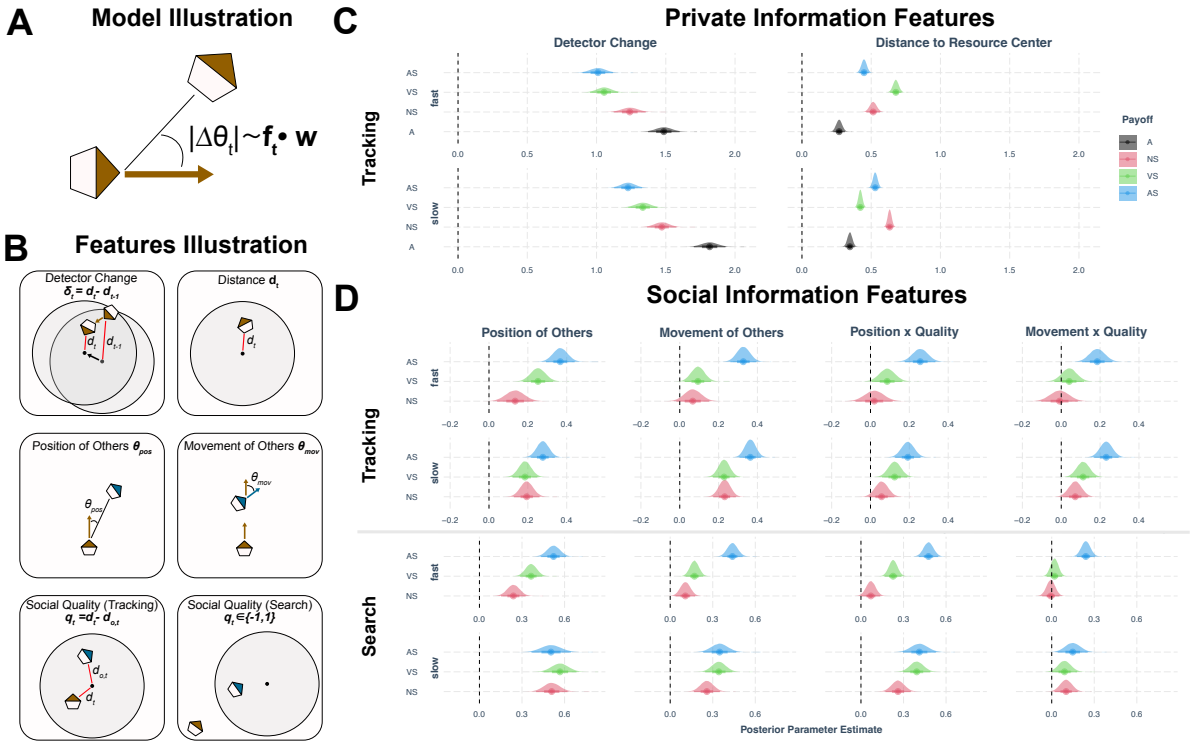

Figure 4: Computational model of movement decisions. **(A)** Schematic model illustration predicting the absolute rotation magnitude at each point in time based on a linear combination of dynamic private and social features. **(B)** Illustration of the private and social features used in the model. **(C)** Mean posterior estimates (including 90% HPDIs) per payoff-sharing and resource condition for private information features. **(D)** Mean posterior estimates (including 90% HPDIs) per payoff-sharing and resource condition for social information features.

A mechanistic agent-based simulation

To confirm that payoff selectivity was the key factor determining collective outcomes and to gain generalizable insights beyond the two resource environments studied in the experiment, we developed a mechanistic agent-based simulation of the task. At each simulation time step, agents

decided on their next movement direction based on either private or social information, with the social probability (p_{social}) depending on the quality of available social cues (i.e., the difference in current payoffs between agents and observed others), and their selectivity in responding to those cues (Fig. 5A). High selectivity meant that agents only used social information if others were doing better than they were at the time. If agents followed social information, they compromised between their previous movement direction and the average position of others. When agents instead relied on private information (with probability $1 - p_{\text{social}}$), they followed the heuristic identified before (see Figs. 1D and 2B): They continued in the same direction if they were approaching the resource center and rotated if they moved away from the center (see "Methods" for a detailed description).

Fig. 5B plots tracking time and tracking efficiency for social agents compared to solitary agents (large black dot) across a range of resource speeds (shape) and degrees of selectivity (color). Unsurprisingly, agents that were highly selective in their social information use spent more time on the resource and had a higher tracking efficiency. While agents in groups outperformed singletons across a broad range of selectivity values in terms of tracking time, only highly selective social agents outperformed singletons in terms of tracking efficiency. The costs and benefits of sociality were also modulated by the speed of the resource. In fast-moving environments (80% and 100% of agents' speed), social agents spent slightly more time on the resource compared to singletons, with only small effects of selectivity. In slow-moving environments (20% and 40% of agents' speed), selectivity had a much greater influence on tracking time: Social agents spent either less or substantially more time on the resource compared to singletons, depending on the degree of selectivity. Crucially, social agents outperformed singletons in both tracking time and efficiency only when the resource moved at a moderately slow pace (40% of agents' speed) and when social information was used selectively.

These simulation results largely match our experimental findings, and help explain them in more detail. In our experimental slow-moving environment (with the resource moving at 40% of agents' speed), participants in FP groups outperformed singletons in both performance metrics (Fig. 2A), providing a direct match with the only resource speed at which this is predicted to happen for highly selective agents. In the simulation, relatively non-selective social agents could also spend more time on the resource than singletons, confirming the empirical finding that—at least in slow environments—participants in NP and VP groups outperformed the tracking time of singletons. However, non-selective agents could not match the tracking efficiency of singletons either empirically or in the simulation. Additional simulations (see Supplementary Information Section S8 and Fig. S20) showed that the benefits of selectivity were strongest for imperfect individual trackers. This result suggests that selective social learning is particularly consequential when private cues are unreliable or ambiguous. Agents with high detector sensitivity performed well with less-selective social strategies, indicating that strong reliance on private information could mitigate the risks of maladaptive social influence.

Discussion

Flexible social learning is often a shortcut to better decision making. It underlies humans' collective adaptability and, ultimately, our success as a species (Henrich & McElreath, 2003;

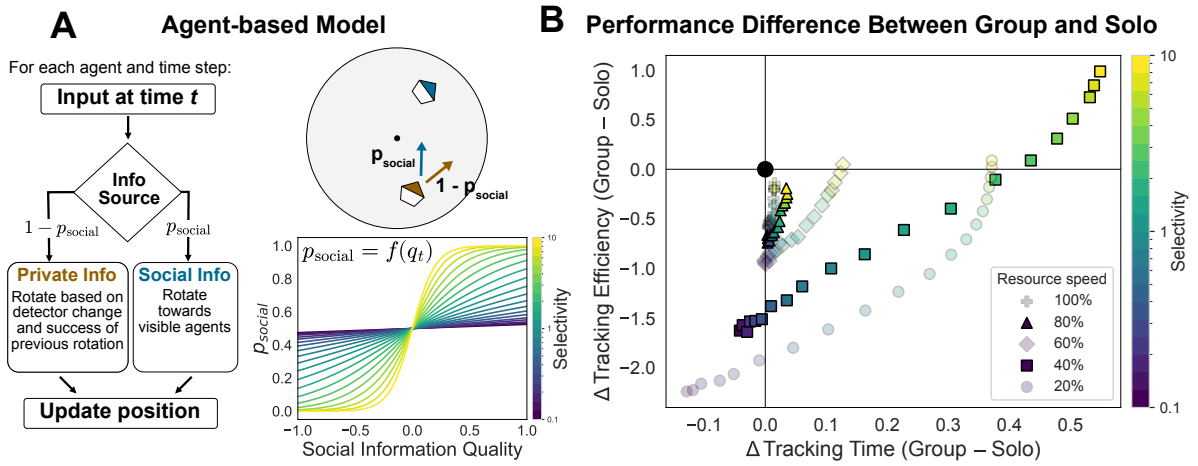

Figure 5: Agent-based simulation results. (A) Model illustration: At each time step, agents rotate based on either private information (with probability $1 - p_{\text{social}}$) or social information (with probability p_{social}). Probability of acting based on social information (p_{social}) depends on social information quality (q_t). If agents followed social information, they rotated towards the center of the locations of other agents in their field of view. If they followed private information, the rotation magnitude was proportional to the change in detector value (δ_t) and the rotation direction depended on the outcome of the previous rotation. **Bottom right**: Agents' selectivity to social information quality; colored lines represent degrees of selectivity. Highly selective agents (yellow) only followed social information if agents in their field of view were performing better than they were at the time; non-selective agents (blue) followed others independently of quality. **(B)** Average tracking time vs. tracking efficiency of groups relative to solitary agents (black dot). Colors show selectivity levels; opaque points correspond to the two experimental speeds (40% and 80%).

Kendal et al., 2018b; Galesic et al., 2023). Yet little is known about how collective intelligence emerges in naturalistic mobile human groups dealing with dynamically changing environments. There is also limited knowledge of how people in such complex tasks integrate dynamic personal and social features, and how these strategies interact with environments, leading to adaptive or maladaptive collective outcomes.

Our immersive-reality experiment shows that groups can outperform singletons in such complex environments, under specific conditions: Only when participants could observe others' payoffs continuously did groups outperform singletons. Contrasting previous findings from the collective-sensing literature in animals (Berdahl et al., 2013) and in humans using more abstract experiments (Hawkins et al., 2023), groups performed worse than singletons when they only had access to the locations of others—especially when tracking a fast-moving resource. Visibility network analysis and computational modeling confirmed that these differences in collective outcomes stem from the way people balance private and social cues, with full payoff information allowing for rapid reconfiguration of visibility networks and selective tuning of social information use.

To be successful in our paradigm, participants needed to find efficient strategies for both searching the resource and tracking its center. Our analysis reveals that payoff selectivity is key for both components of adaptive behavior. During the search phase, when a participant discovered the resource, payoff information allowed groups to flexibly adjust their visual connections and orient themselves towards the discoverer, enabling them to rapidly converge on the resource location (Almaatouq et al., 2020). In contrast, without reliable payoff information, resource discoveries went mostly unnoticed by other group members, making it impossible to

reap the collective benefits of costly search (Mezey et al., 2024). During the tracking phase, payoff information allowed participants to flexibly exploit social information, relying on others' behavior only when it provided adaptive information. In fact, payoff selectivity allowed participants in groups to achieve a higher tracking efficiency compared to solitary individuals (Fig. 2A), while being less sensitive to otherwise essential private information about changes in reward rates (Fig. 4C). They did this by following both the locations and movement directions of others, primarily when group members were better positioned than they were. Because, unlike previous experiments, our task involved an inherent trade-off between private and social information use, following others without a quality filter backfired in groups without reliable payoff information, lowering their performance compared to singletons. Moreover, this maladaptive overuse of social information was amplified by greater environmental volatility: Since the resource location moved faster, positional cues were no longer reliable predictors of future resource locations, whereas visible payoffs still provided real-time information on the environmental target, thereby ensuring collective adaptation even in rapidly changing conditions.

Our agent-based simulations not only confirmed the decisive role of payoff selectivity for collective performance, they also clarified the role of the environment. During search, when private information is absent, low-quality social information also provides beneficial hints about resource location, resulting in collective improvements in tracking time (i.e., time on the resource) across a wide range of environments. During tracking, participants need to strategically balance private detector feedback and social cues, limiting the environments in which social information—even if used selectively—is beneficial. When the resource moves slowly, private information is sufficient for tracking the resource and social cues offer little additional value. When the resource moves quickly, on the other hand, reliance on potentially outdated social cues at the expense of private information impairs tracking and frequently leads to losing the resource. Between those extremes lies an ecological "sweet spot"—corresponding to the slow-resource condition in the experiment—where social information use not only benefits searching but also tracking the resource. Because private cues can be ambiguous and mapping observed detector changes to optimal movement decisions can be cognitively demanding, simply copying high-performing neighbors overcomes this deficiency and increases performance beyond the level of singletons.

Future work could systematically vary group size, which proved important for collective-foraging dynamics in simulations (Beauchamp, 2008; Mezey et al., 2024), in order to investigate how the costs and benefits of social information use across environments might change as groups become larger. Moreover, we only considered groups of identical agents. Systematically examining the role of individual heterogeneity within groups—both synthetic and human—may reveal a more complex picture of the optimality and trade-offs that individuals face in collective search and tracking. Importantly, by showcasing a way of studying human behavior beyond the highly constrained paradigms often used in cognitive science, psychology, and economics, our work also paves the way towards analyses of collective human adaptation outside of the lab, for example, during social foraging (Schakowski et al., 2025).

In line with simulation work predicting that unconditional payoff sharing can evolve by recruiting group members as potentially useful sources of social information (Tump et al., 2019), results from the Voluntary Payoff-Sharing condition showed that participants were indeed willing to pay a personal cost to actively share payoff information with others. This active payoff

sharing not only resulted in more adaptive visual information flow following resource discoveries and more selective tuning of social information use, but also improved overall performance compared to groups without the ability to share payoffs. Future work could explore sharing tendencies in groups of different sizes—simulations predict unconditional sharing to decline in larger groups (Tump et al., 2019)—and further elucidate the underlying decision rules of active payoff sharing. Is payoff sharing driven by reciprocity, normative pressures within the group, or stable altruistic tendencies? To isolate these motives, our experimental design could be adjusted to tease apart competing mechanisms. Intriguingly, collective foraging has recently been posited as a powerful framework to model the evolution of prosocial communication and human language (Cambier et al., 2024), generating predictions that can be tested using our framework.

Our study demonstrates that collective intelligence does not automatically emerge under naturalistic conditions as soon as multiple individuals are grouped together—instead, it depends on the specific way that personal and social cues are integrated and is sensitive to environmental volatility. By combining behavioral and dynamic visibility-network analyses with fine-grained computational modeling and agent-based simulations, we provide multiple complementary lines of evidence identifying payoff selectivity as the key driver of collective intelligence in spatial search and tracking. These findings pinpoint the conditions under which shared information transforms a group of individuals into an intelligent collective, and pave the way for future investigations of social interactions in naturalistic groups.

Methods

Participants and design

This research complies with all relevant ethical regulations and was approved by the Institutional Review Board of the Max Planck Institute for Human Development (number: A 2022-26). We recruited 796 participants online from Prolific (aged 18–65 years, with a minimum Prolific approval rate of 95%), who provided informed consent before starting the experiment. We removed participants who did not complete the experiment ($n = 21$); who had a very low frame rate ($> 5\%$ below the target of 10 Hz), causing faulty rendering of the environment ($n = 27$); who did not move for more than 25% of the experiment ($n = 29$); who were assigned to group conditions but could not be matched within 10 min ($n = 59$); and who were in groups with more than one invalid participant ($n = 39$). This resulted in a final sample size of 621 (female: 239; male: 381; prefer not to say: 1; M_{age}= 33.56, SD_{age} = 10.17; see Supplementary Table 1 for an overview of the number of participants for each of the eight conditions). Participants earned a baseline of £3 for completing the study and could earn a bonus of up to £2 based on their individual performance (i.e., total score). Participants in the top 10% of performance within each condition received a £2 bonus, participants in the 10–50% range received a £1 bonus, and participants in the 50–75% range received a £0.50 bonus. Our preregistration is accessible at `https://aspredicted.org/C62_M6Z`.

Participants completed 15 min of the task in a 4×2 between-subjects design (Fig. 1C; see Supplementary Information Section S3 for details on assignment procedures and dates of data collection). Participants were allotted to one of four payoff conditions, completing the task by themselves (*Alone*, A), in groups where others' locations but not payoffs were available (*No*

Payoff-Sharing, NP), in groups where others' payoffs were also available (*Full Payoff-Sharing*, FP), or in groups where participants could decide whether to share their payoff information (*Voluntary Payoff-Sharing*, VP). In the NP condition, participants could observe and interact with their group members in real time, but could not see how many points they were currently collecting. In the FP condition, they could also observe their group members' current payoffs (indicated by a colored beam above avatars; see Fig. 1). Participants could thus directly observe the resource quality at each group member's location, provided they were in their field of view. In the VP condition, participants could continuously decide whether they wanted to share their current payoff information or not at a cost of 1 point per second.

Participants were tasked to search and track either a slow or fast resource. The slow resource was fairly easy to follow: It moved at 2.8 m/s, corresponding to 40% of participants' speed. The fast resource was fairly difficult to follow: It moved at 5.6 m/s, corresponding to 80% of participants' speed. The resource movement followed a Lévy walk, with step lengths drawn from a power-law distribution with a shape parameter $\alpha = 1$ (limited to steps between 1 and 100 m), and movement directions sampled from a uniform distribution. If the resource center approached the boundary of the environment, the movement direction was resampled. Qualitatively, resource movement consisted of frequent short steps and infrequent long steps (an example of a resource movement trajectory is available at `https://youtu.be/pHE5aOMb1_M` or as Video 1 in the supplementary materials).

Experimental procedure

After reading the instructions and passing comprehension checks, participants completed a tutorial to familiarize themselves with the task and controls. Participants in group conditions then entered a virtual waiting room in order to be matched with other participants. The experiment started after a group of five was formed. Participants who could not be matched within 10 min were financially compensated and removed from the experiment.

In the experiment, participants were immersed in a 3D environment, freely navigating an astronaut avatar from a first-person perspective (90° horizontal and 60° vertical field of view) through a circular crater on a distant planet (400 m diameter; see Fig. 1 and videos of the experiment at `https://youtu.be/AcfIw_qWR_Q` and `https://youtu.be/xY7nzh4vF4o`, or Videos 2 and 3 in the supplementary materials).

Participants could move left, forward, or right using the "A," "W," and "D" keys, respectively, or using the corresponding arrow keys. They could move at 7 m/s and rotate at 150°/s, and were instructed to locate and track a hidden, mobile resource in order to collect points and maximize their bonus payment. The resource was circular and had a 40 m radius, yielding a payoff of 40 points/s in the center, linearly decreasing to one point/s at the edge. Avatars held a resource detector indicating the resource quality (i.e., payoff) at their current location (Fig. 1B). Movement towards the resource center was indicated by increasingly higher values and deeper reds on the resource detector. At the beginning of the experiment, the resource was placed in the center of the arena and participants were initialized on the resource facing its center.

The study was implemented using the Unity game engine, version 2021.3.14f1 (Unity Technologies, 2021) and compiled to run in a web browser using `WebGL` technology. `PlayFab` (Mi-

crosoft Corporation, 2023) provided the game server responsible for synchronizing the participants. Communication between the client and the server was handled by the `Mirror` Unity package (Vis2K, 2023). Participant data was recorded locally and uploaded to the `PlayFab` server at the end of the experiment for the alone condition. For the group conditions, data was recorded on the `PlayFab` game server, alongside the resource traces.

Data

At a sampling interval of 10 Hz, we recorded the positions (i.e., x- and z-coordinates) of the resource center and participants' avatars, the rotations (around the y-axis) of participants' avatars, the scores that participants received at each time step, and whether or not the participants were sharing their payoffs at that moment (in the Voluntary Payoff-Sharing condition). From this raw data, we reconstructed the movement trajectories and visual information of each participant using `Python 3.9` (Van Rossum & Drake, 2009) and Python libraries `numpy` (Harris et al., 2020), `pandas` (McKinney, 2010), and `xarray` (Hoyer & Hamman, 2017).

Data analysis

Behavioral analyses

To quantify how participants' performance differed among experimental conditions while also accounting for participant- and group-level variability, we applied multilevel Bayesian Beta regression models to our three performance measures: tracking time, tracking efficiency, and total number of points. Tracking time represents the proportion of time participants spent on the resource. Tracking efficiency was calculated as the average number of points collected when participants were on the resource.

Dynamic visibility network analysis

To analyze the structure of social interactions, we constructed dynamic visibility networks for each group at each one-second interval. A participant j was considered visible to participant i if j was within i's 90° forward-facing field of view. This condition is met if the absolute angular difference between participant i's heading direction (θ_i) and the angle towards participant j ($\theta_{i\to j}$) is less than 45°:

$$|\theta_{i\to j} - \theta_i| < 45°.$$

The angle from i to j is calculated from their respective positions, $\mathbf{p}_i = (x_i, y_i)$ and $\mathbf{p}_j = (x_j, y_j)$, as:

$$\theta_{i\to j} = \text{atan2}(y_j - y_i, x_j - x_i).$$

This pairwise check for all participants at each time step generated a directed graph (a dynamic network), where nodes represent participants and a directed edge from i to j indicates that i could see j. From these networks, we computed two key metrics for each participant at each time step: *in-degree* (the number of individuals observing them) and *out-degree* (the

number of individuals they observed). These networks were constructed and analyzed using the `NetworkX` Python package (Hagberg et al., 2008).

To analyze overall network connectivity (Fig. 3A) we applied a Bayesian Poisson regression; to analyze adaptive connectivity (Fig. 3B) we applied a Bayesian logistic regression, in both cases accounting for individual- and group-level heterogeneity.

Resource discovery events. To investigate the temporal dynamics of visibility network adaptation, we analyzed resource discovery events in which one group member, the "discoverer," discovers the resource while the other group members are searching for it (Fig. 3C). These events were characterized by a specific set of conditions: all group members were searching (i.e., were not on the resource) for at least 5 s, and exactly one participant entered the resource and stayed on it for at least 5 s. For these events, we analyzed changes in visibility and performance in the 30 s following the resource discovery event (see Fig. S10 for an illustration). In case of overlapping events, only the first event was used. We used Gaussian process function learning through the `gp` function in `brms` (Bürkner, 2018) to estimate how visibility networks and performance changed over time for the "discoverer" and for "others."

Computational model of rotation decisions

To better understand individual movement decisions at a mechanistic level, we developed a computational modeling framework that sequentially predicts participants' movement decisions based on a linear combination of private and social information features. Movement decisions consist of two components: rotation direction (whether participants turn clockwise or counter-clockwise) and rotation magnitude (how strongly they adjust their direction). We present the analysis of rotation direction in the Supplementary Information Section S6; in the main text, we focus on rotation magnitude, which can be expressed more directly in relation to private and social information features. Although behavior was recorded at 10 Hz, for modeling purposes we discretized it into 1 s intervals. At each interval, the absolute rotation magnitude is modeled as

$$|\Delta\theta_t| \sim \text{Exponential}(\lambda_t), \qquad \log \lambda_t = w_0 + \mathbf{f}_t^\top \mathbf{w},$$

where $\mathbf{f}_t$ represents the vector of private and social features observed at time t and $\mathbf{w}$ denotes the corresponding feature weights. The components of $\mathbf{f}_t$ are introduced in the following subsections. The model assumes that participants integrate both types of information to decide how much to deviate from their current movement direction. This framework allows us to quantify the relative influence of different, dynamically changing private and social cues across experimental conditions (see Fig. 4 for illustrations).

Private information features. The private information features capture how participants responded to changes in their own detector readings and positions relative to the resource. These features were only present during tracking phases.

The first private information feature is the detector change (δ_t), which represents the change

in distance to the resource center between consecutive time steps:

$$\delta_t = d_t - d_{t-1},$$

where d_t is the detector value (distance to the resource center) at time t. A negative detector change ($\delta_t < 0$) indicates a decrease in distance (i.e., moving closer to the resource), while a positive detector change ($\delta_t > 0$) indicates an increase in distance (i.e., moving away from the resource). According to our analytical derivation, optimal trackers should rotate more if their detector change indicates movement away from the resource center and less if the detector indicates movement towards the center (see Supplementary Information Section S4). This feature is thus critical for tracking across experimental conditions, as it directly informs participants about performance.

The second private feature is the absolute distance to the resource center (d_t). This feature does not provide additional directional information, but it can still influence behavior, as indicated by the behavior rotation analysis (Fig. 2B).

Social information features. The model also incorporates a set of social features that participants might use in both tracking and search phases. These features are calculated based on the average position and average direction of motion of others within the focal participant's field of view.

The first social feature is the position of others ($\theta_{\text{pos},t}$), representing the angular difference between the focal participant's heading direction and the average position of others within the field of view:

$$\theta_{\text{pos},t} = |\theta_{\text{group},t} - \theta_t|,$$

where θ_t is the current heading direction of the focal participant and $\theta_{\text{group},t}$ is the angle towards the average position of visible others. Letting the participant's position be $\mathbf{p}_t = (x_t, y_t)$ and the average position of the N visible others be $(\bar{x}_t, \bar{y}_t)$, this angle is calculated as

$$\theta_{\text{group},t} = \text{atan2}(\bar{y}_t - y_t, \bar{x}_t - x_t),$$

Larger values indicate that others are positioned at a larger angle from the current direction of motion of the focal participant. If participants use this feature, they rotate less when others are near the center of their field of view and more when others are toward the periphery of their field of view.

The second social feature is the movement direction of others ($\theta_{\text{mov},t}$), reflecting the angular difference between the focal participant's heading direction and the average movement direction of others in the field of view:

$$\theta_{\text{mov},t} = |\bar{\theta}_{m,t} - \theta_t|,$$

where $\bar{\theta}_{m,t}$ is the average movement direction of others in the field of view at time t. Large values indicate that others are moving against the focal participant's current direction, while small values indicate that others are moving in the same direction as the focal participant. This feature might serve as a proxy for others' beliefs about the location of the resource, as the observer can infer the assumed location of the resource center based on the direction others are moving in.

Social information quality. To investigate how social information quality influences participants' reliance on social cues across conditions, we included interactions of both social features with social information quality. For tracking, relative social information quality (q_t) is defined as

$$q_t = d_t - \bar{d}_{o,t},$$

where d_t represents the participant's distance from the resource center and $\bar{d}_{o,t}$ represents the average distance of others within the participant's field of view from the resource center. Positive values ($q_t > 0$) indicate that others are closer to the resource center, while negative values ($q_t < 0$) indicate that others are farther away from the resource center.

For searching, relative social information quality is represented as a binary variable,

$$q_t \in \{-1, 1\},$$

where $q_t = 1$ indicates that the average position of others in the focal participant's field of view is on the resource at time t, and $q_t = -1$ indicates they are not.

Note that social information quality could only be directly and consistently accessed in the FP experimental condition (via the colored beam). In the NP condition it had to be inferred.

To ensure that shared feature weights could be interpreted across conditions and to facilitate model convergence, all features were normalized to a range between $[-1, 1]$.

Model fitting

All models were fitted in a Bayesian framework using Hamiltonian Monte Carlo in Stan (Carpenter et al., 2017), implemented in R version 4.2.1 with the `brms` package (Bürkner, 2018). We used weakly informative—or non-informative—priors for all parameters. Posterior predictive checks and visual inspection of the trace plots confirmed model convergence. We report the posterior means and 90% highest posterior density intervals (HPDIs) of the differences between conditions (i.e., contrasts) using `tidybayes` (Kay, 2023) and `emmeans` (Lenth et al., 2023) R packages following Heiss (2021). The `tidyverse` (Wickham et al., 2019) packages were used for performing data manipulation and generating the final visualizations.

Agent-based simulation

To link the identified mechanisms to the observed collective dynamics and extend our results beyond the specific settings of the experiment, we developed an agent-based simulation, mirroring the structure of the experiment. In the simulations, agents are assumed to search for and track a mobile resource, which moves according to the same Lévy-walk process used in the experiment.

Agents are assumed to move at a constant speed v, updating their position $\mathbf{p}_{t+1}$ at each time step t based on their heading angle θ_t:

$$\mathbf{p}_{t+1} = \mathbf{p}_t + v \cdot \Delta t \cdot \begin{pmatrix} \cos(\theta_t) \\ \sin(\theta_t) \end{pmatrix},$$

where $\mathbf{p}_t = (x_t, y_t)$ is the position at time t, and Δt is the time step duration. During tracking

(i.e., when both private and social information is available), the agent's new heading angle θ_{t+1} is determined based on its current heading θ_t and a chosen orientation change $\Delta\theta_t$:

$$\theta_{t+1} \sim \mathcal{N}(\theta_t + \Delta\theta_t, \sigma^2)$$

where $\sigma = 10°$, and $\Delta\theta_t$ is chosen probabilistically between social and private information:

$$\Delta\theta_t = \begin{cases} \Delta\theta_t^{\text{social}}, & \text{if } R < p_{\text{social}}, \\ \Delta\theta_t^{\text{private}}, & \text{if } R \geq p_{\text{social}}, \end{cases}$$

where $R \sim U(0,1)$, $\Delta\theta_t^{\text{social}}$, and $\Delta\theta_t^{\text{private}}$ are the agent's orientation change based on social and private information respectively.

For private information, the agent first determines the magnitude of rotation, $\Delta\theta_t^{\text{private (mag)}}$, based on the change in distance to the resource, $\delta_t = d_t - d_{t-1}$,:

$$\Delta\theta_t^{\text{private (mag)}} = \beta_0 + \beta_1\delta_t,$$

where β_1 controls sensitivity to the change in distance and β_0 is the baseline rotation magnitude. For all simulations $\beta_0 = \max(\beta_1, 50°)$. The agent then decides whether to continue turning in the same direction or reverse. The probability of reversing direction, $p_{\text{change direction}}$,

$$p_{\text{change direction}} = \begin{cases} p_{\text{success}}, & \text{if } \delta_t < \delta_{t-1}, \\ p_{\text{failure}}, & \text{if } \delta_t \geq \delta_{t-1}, \end{cases}$$

so that the final orientation change, $\Delta\theta_t^{\text{private}}$, is determined:

$$\Delta\theta_t^{\text{private}} = \begin{cases} -\text{sgn}(\Delta\theta_{t-1}) \cdot \Delta\theta_t^{\text{private (mag)}}, & \text{if } R_2 < p_{\text{change direction}}, \\ \text{sgn}(\Delta\theta_{t-1}) \cdot \Delta\theta_t^{\text{private (mag)}}, & \text{if } R_2 \geq p_{\text{change direction}}, \end{cases}$$

where $R_2 \sim U(0,1)$, $p_{\text{success}} = 0.15$ and $p_{\text{failure}} = 0.35$ based on the human behavioral results (see Supplementary Information Section S6), and $\Delta\theta_{t-1}$ is the net orientation change from the previous time step.

Social information biases the rotation of an agent towards the average position of its visible neighbors. The probability of using social information p_{social} is calculated using a logistic function of the relative quality of social information q_t:

$$p_{\text{social}} = \frac{1}{1 + \exp(-k(q_t))},$$

where k controls selectivity to social information quality, and q_t is calculated by comparing the agent's own distance to the resource with the average distance of its visible neighbors:

$$q_t = d_t - \bar{d}_{o,t}$$

Here, d_t is the focal agent's distance to the resource at time t, and $\bar{d}_{o,t}$ is the average distance of visible neighbors to the resource. A positive q_t indicates the agent is farther from the resource than its neighbors, making social information more valuable.

Orientation change based on social information is defined by the difference between the agent's current heading direction θ_t and the angle towards the average location of other agents in its field of view, $\theta_{\text{group},t}$:

$$\Delta\theta_t^{\text{social}} = \theta_{\text{group},t} - \theta_t$$

As in the experiment, the field of view is set to 90°.

When searching (i.e., when no private information is available), agents follow a socially biased correlated random walk influenced by social information within their field of view. Social information is treated similarly to tracking, except that the relative quality of social information (q_t) is binarized based on whether others are on the resource ($q_t = 1$) or not ($q_t = -1$), as in the computational model. When not acting based on social information, the rotation magnitude is uniformly sampled from $U(0, r_{\max})$ and the direction is randomly chosen. Here, $r_{\max}$ represents the maximum rotation at each time step when the agent was searching and is set to $r_{\max} = 90°$ for all simulations.

Data and code availability

Raw time series data, metadata, processed tables of computed measures, and all analysis code are available on the Open Science Framework (https://osf.io/zrhwt/). An online tool is available to visualize the raw time series data (https://vagechirkov.github.io/CollectiveSearchOnMarsTraceViewer/).

References

Almaatouq, A., Noriega-Campero, A., Alotaibi, A., Krafft, P. M., Moussaid, M., & Pentland, A. (2020). Adaptive social networks promote the wisdom of crowds. *Proceedings of the National Academy of Sciences*, 117(21), 11379–11386.

Bastien, R. & Romanczuk, P. (2020). A model of collective behavior based purely on vision. *Science advances*, 6(6), eaay0792.

Beauchamp, G. (2008). A spatial model of producing and scrounging. *Animal Behaviour*, 76(6), 1935–1942.

Berdahl, A., Torney, C. J., Ioannou, C. C., Faria, J. J., & Couzin, I. D. (2013). Emergent Sensing of Complex Environments by Mobile Animal Groups. *Science*, 339(6119), 574–576.

Bürkner, P.-C. (2018). Advanced Bayesian Multilevel Modeling with the R Package brms. *The R Journal*, 10(1), 395.

Cambier, N., Miletitch, R., Benítez-Burraco, A., & Raviv, L. (2024). Pros and cons of prosociality across ecological niches: a swarm robotics approach. *Research Square*.

Caraco, T. (1981). Risk-sensitivity and foraging groups. *Ecology*, 62(3), 527–531.

Carpenter, B., Gelman, A., Hoffman, M. D., Lee, D., Goodrich, B., Betancourt, M., Brubaker, M., Guo, J., Li, P., & Riddell, A. (2017). Stan: A Probabilistic Programming Language. *Journal of Statistical Software*, 76, 1–32.

Deffner, D., Kleinow, V., & McElreath, R. (2020). Dynamic social learning in temporally and spatially variable environments. *Royal Society open science*, 7(12), 200734.

Deffner, D., Mezey, D., Kahl, B., Schakowski, A., Romanczuk, P., Wu, C. M., & Kurvers, R. H. (2024). Collective incentives reduce over-exploitation of social information in unconstrained human groups. *Nature Communications*, 15(1), 2683.

Galesic, M., Barkoczi, D., Berdahl, A. M., Biro, D., Carbone, G., Giannoccaro, I., Goldstone, R. L., Gonzalez, C., Kandler, A., Kao, A. B., et al. (2023). Beyond collective intelligence: Collective adaptation. *Journal of the Royal Society Interface*, 20(200), 20220736.

Garg, K., Deng, W., & Mobbs, D. (2024). Beyond the individual: A social foraging framework to study decisions in groups.

Hagberg, A. A., Schult, D. A., & Swart, P. J. (2008). Exploring Network Structure, Dynamics, and Function using NetworkX. *scipy*.

Harris, C. R., Millman, K. J., Van Der Walt, S. J., Gommers, R., Virtanen, P., Cournapeau, D., Wieser, E., Taylor, J., Berg, S., Smith, N. J., Kern, R., Picus, M., Hoyer, S., Van Kerkwijk, M. H., Brett, M., Haldane, A., Del Río, J. F., Wiebe, M., Peterson, P., Gérard-Marchant, P., Sheppard, K., Reddy, T., Weckesser, W., Abbasi, H., Gohlke, C., & Oliphant, T. E. (2020). Array programming with NumPy. *Nature*, 585(7825), 357–362.

Hawkins, R. D., Berdahl, A. M., Pentland, A. S., Tenenbaum, J. B., Goodman, N. D., & Krafft, P. M. (2023). Flexible social inference facilitates targeted social learning when rewards are not observable. *Nature Human Behaviour*, (pp. 1–10).

Hein, A. M., Rosenthal, S. B., Hagstrom, G. I., Berdahl, A., Torney, C. J., & Couzin, I. D. (2015). The evolution of distributed sensing and collective computation in animal populations. *eLife*, 4.

Heiss, A. (2021). A guide to correctly calculating posterior predictions and average marginal effects with multilievel Bayesian models.

Henrich, J. & McElreath, R. (2003). The evolution of cultural evolution. *Evolutionary Anthropology: Issues, News, and Reviews: Issues, News, and Reviews*, 12(3), 123–135.

Heyes, C. (2016). Blackboxing: social learning strategies and cultural evolution. *Philosophical Transactions of the Royal Society B: Biological Sciences*, 371(1693), 20150369.

Hoyer, S. & Hamman, J. (2017). Xarray: N-D labeled Arrays and Datasets in Python. *Journal of Open Research Software*, 5(1), 10.

Kay, M. (2023). Tidybayes: Tidy Data and Geoms for Bayesian Models. Zenodo.

Kendal, R. L., Boogert, N. J., Rendell, L., Laland, K. N., Webster, M., & Jones, P. L. (2018a). Social Learning Strategies: Bridge-Building between Fields. *Trends in Cognitive Sciences*, 22(7), 651–665.

Kendal, R. L., Boogert, N. J., Rendell, L., Laland, K. N., Webster, M., & Jones, P. L. (2018b). Social learning strategies: Bridge-building between fields. *Trends in cognitive sciences*, 22(7), 651–665.

Laland, K. N. (2004). Social learning strategies. *Animal Learning & Behavior*, 32(1), 4–14.

Lenth, R. V., Bolker, B., Buerkner, P., Giné-Vázquez, I., Herve, M., Jung, M., Love, J., Miguez, F., Riebl, H., & Singmann, H. (2023). Emmeans: Estimated Marginal Means, aka Least-Squares Means.

McKinney, W. (2010). Data Structures for Statistical Computing in Python. *Proceedings of the 9th Python in Science Conference*, (pp. 56–61).

Mezey, D., Deffner, D., Kurvers, R. H., & Romanczuk, P. (2024). Visual social information use in collective foraging. *PLOS Computational Biology*, 20(5), e1012087.

Microsoft Corporation (2023). Playfab documentation. Game backend services.

Puckett, J. G., Pokhrel, A. R., & Giannini, J. A. (2018). Collective gradient sensing in fish schools. *Scientific Reports*, 8(1), 7587.

Rahmani, P., Peruani, F., & Romanczuk, P. (2020). Flocking in complex environments—attention trade-offs in collective information processing. *PLoS computational biology*, 16(4), e1007697.

Schakowski, A., Deffner, D., Kortet, R., Niemelä, P. T., Kavelaars, M. M., Monk, C. T., Pykälä, M., & Kurvers, R. H. (2025). Socioecology drives adaptive social foraging dynamics in the wild. *OSF*.

Schultner, D., Molleman, L., & Lindström, B. (2025). Feature-based reward learning shapes human social learning strategies. *Nature Human Behaviour*, (pp. 1–16).

Toyokawa, W., Whalen, A., & Laland, K. N. (2019). Social learning strategies regulate the wisdom and madness of interactive crowds. *Nature Human Behaviour*, 3(2), 183–193.

Tump, A. N., Deffner, D., Pleskac, T. J., Romanczuk, P., & M. Kurvers, R. H. (2024). A cognitive computational approach to social and collective decision-making. *Perspectives on Psychological Science*, 19(2), 538–551.

Tump, A. N., Pleskac, T. J., & Kurvers, R. H. (2020). Wise or mad crowds? the cognitive mechanisms underlying information cascades. *Science Advances*, 6(29), eabb0266.

Tump, A. N., Wu, C. M., Bouhlel, I., & Goldstone, R. L. (2019). *The Evolutionary Dynamics of Cooperation in Collective Search*. Preprint, Animal Behavior and Cognition.

Unity Technologies (2021). *Unity Game Engine Documentation*. Version 2021.3.14f1, built-in rendering pipeline.

Van Rossum, G. & Drake, F. L. (2009). *Python 3 Reference Manual*. Scotts Valley, CA: CreateSpace.

Vis2K (2023). Mirror networking for unity. Unity package for multiplayer networking.

Wickham, H., Averick, M., Bryan, J., Chang, W., McGowan, L. D., François, R., Grolemund, G., Hayes, A., Henry, L., Hester, J., Kuhn, M., Pedersen, T. L., Miller, E., Bache, S. M., Müller, K., Ooms, J., Robinson, D., Seidel, D. P., Spinu, V., Takahashi, K., Vaughan, D., Wilke, C., Woo, K., & Yutani, H. (2019). Welcome to the Tidyverse. *Journal of Open Source Software*, 4(43), 1686.

Wu, C. M., Deffner, D., Kahl, B., Meder, B., Ho, M. H., & Kurvers, R. H. (2025). Adaptive mechanisms of social and asocial learning in immersive collective foraging. *Nature Communications*, 16(1), 3539.

Zaburdaev, V., Denisov, S., & Klafter, J. (2015). Lévy walks. *Reviews of Modern Physics*, 87(2), 483–530.

Acknowledgments

We thank Deborah Ain for editing the manuscript. This research has been supported by the Deutsche Forschungsgemeinschaft (DFG, German Research Foundation) under Germany's Excellence Strategy – EXC 2002/1 "Science of Intelligence". The funders had no role in study design, data collection and analysis, decision to publish, or preparation of the manuscript.

Author contributions statement

VC, RHJMK, and DD conceived the experiment. VC performed the experiments, processed the data, analyzed the results and prepared the figures, supervised by RHJMK and DD. VC constructed the agent-based simulations under the supervision of RHJMK, PR, and DD. VC and DD wrote the first draft and all authors reviewed the manuscript.

Competing interests

The authors declare no competing interests.

Supplementary Information for

Payoff selectivity unlocks collective intelligence in naturalistic human groups

Valerii Chirkov[1,2,3*], Ralf H.J.M. Kurvers[1,2], Pawel Romanczuk[2,3] & Dominik Deffner[1,2,4*]

[1]Center for Adaptive Rationality, Max Planck Institute for Human Development, Berlin, Germany
[2]Science of Intelligence Excellence Cluster, Technical University Berlin, Berlin, Germany
[3]Institute for Theoretical Biology, Humboldt University Berlin, Berlin, Germany
[4]Department of Psychology, Marburg University, Marburg, Germany
[*]Corresponding authors: valerii.chirkov@hu-berlin.de; dominik.deffner@uni-marburg.de

Contents of Supplementary Information

S1 Supplementary Figures

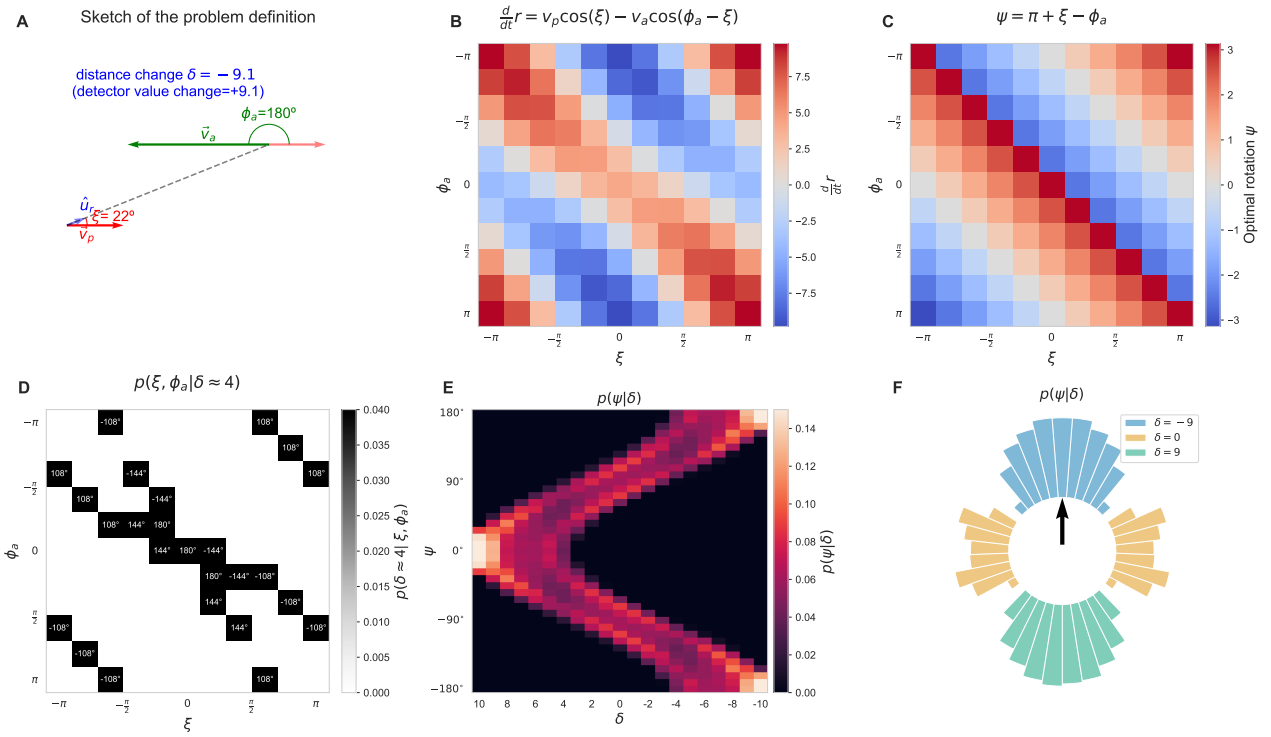

Figure S1: Forward and Inverse Model. **A** Schematic of the forward model's geometry. An agent (velocity $\vec{v}_a$) tracks a moving resource (velocity $\vec{v}_p$). The model is defined in the resource's reference frame, where ϕ_a is the agent's heading relative to the resource's direction of motion, and ξ is the angle of the agent's position relative to that same direction. **B** The forward model output: the rate of change in distance (dr/dt) shown as a function of the agent's relative heading (ϕ_a) and position (ξ). **C** The optimal rotation (ψ) required to intercept the resource, calculated for each combination of ϕ_a and ξ (see Eq. S9). **D** The core ambiguity the inverse model must solve. For a single observed distance change (e.g., $\delta = 4$), multiple combinations of the unknown angles ϕ_a and ξ are possible. Each of these combinations corresponds to a different optimal rotation (values shown in cells). **E** The inverse model's solution: the posterior probability distribution $P(\psi|\delta)$ over all possible rotation angles (y-axis), given distance change δ (x-axis). **F** The same posterior distribution $P(\psi|\delta)$ visualized in polar coordinates for $\delta \in \{-9, 0, 9\}$. All panels are generated using a resource speed of $v_p = 0.4\ v_a$, which corresponds to the slow resource condition in the experiment.

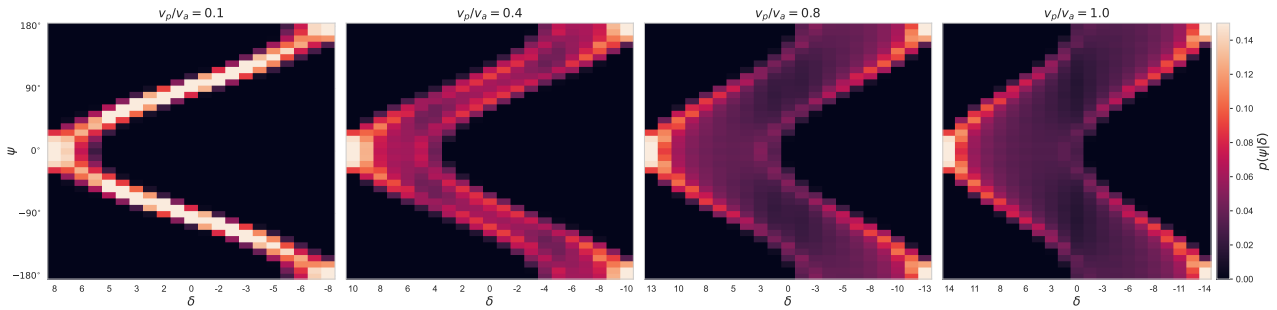

Figure S2: Inference Model $P(\psi|\delta)$ Across Varying Resource Speeds. This figure illustrates the output of the inverse model (posterior probability $P(\psi|\delta)$) for different resource speeds, relative to the agent's speed (v_p/v_a). Panels show the inferred optimal rotation ψ given an observed change in distance δ, when the resource moves at speed: 0.1 v_a, 0.4 v_a, 0.8 v_a, and 1.0 v_a. Each subplot displays the probability distribution over optimal rotations for a range of observed distance changes. As the resource speed increases, the landscape of optimal rotations can become more complex, reflecting the increasing challenge of inferring the correct turn from ambiguous sensory information.

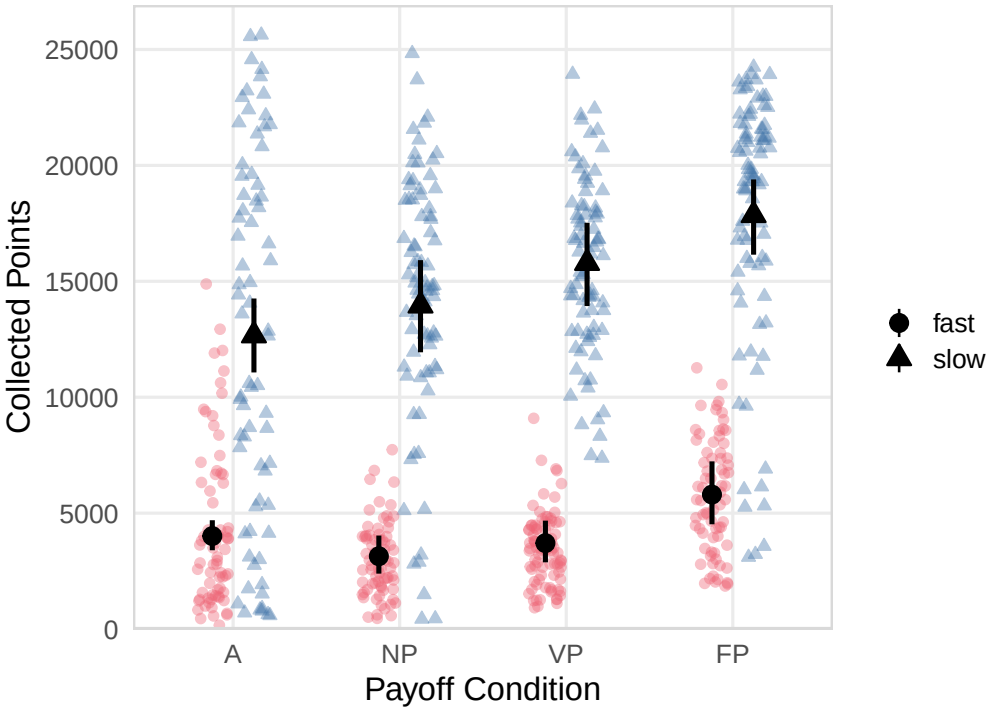

Figure S3: Collected Points. Total number of collected points per treatment, shown for each payoff condition (A: Asocial Condition; NP: No Payoff-Sharing; VP: Voluntary Payoff-Sharing; FP: Full Payoff-Sharing) and resource speed (slow vs. fast). Each dot represents an individual participant. Larger black dots and error bars show posterior means and 90% HPDIs.

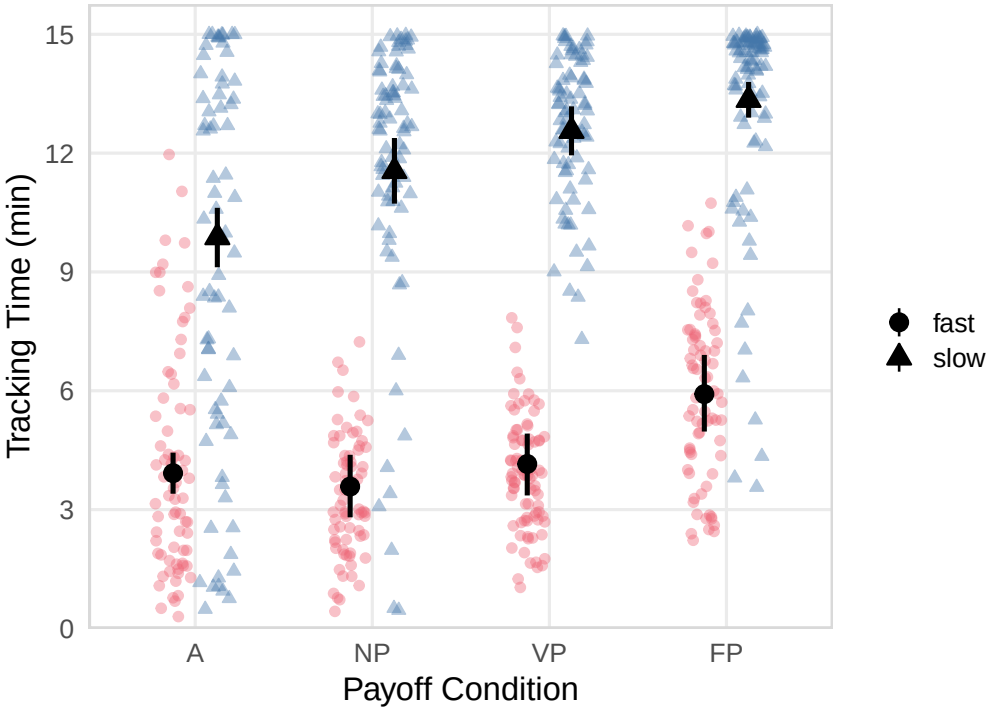

Figure S4: Tracking Time. Mean tracking time in minutes per treatment, shown for each payoff condition (A: Asocial Condition; NP: No Payoff-Sharing; VP: Voluntary Payoff-Sharing; FP: Full Payoff-Sharing) and resource speed (slow vs. fast). Each dot represents an individual participant. Larger black dots and error bars show posterior means and 90% HPDIs.

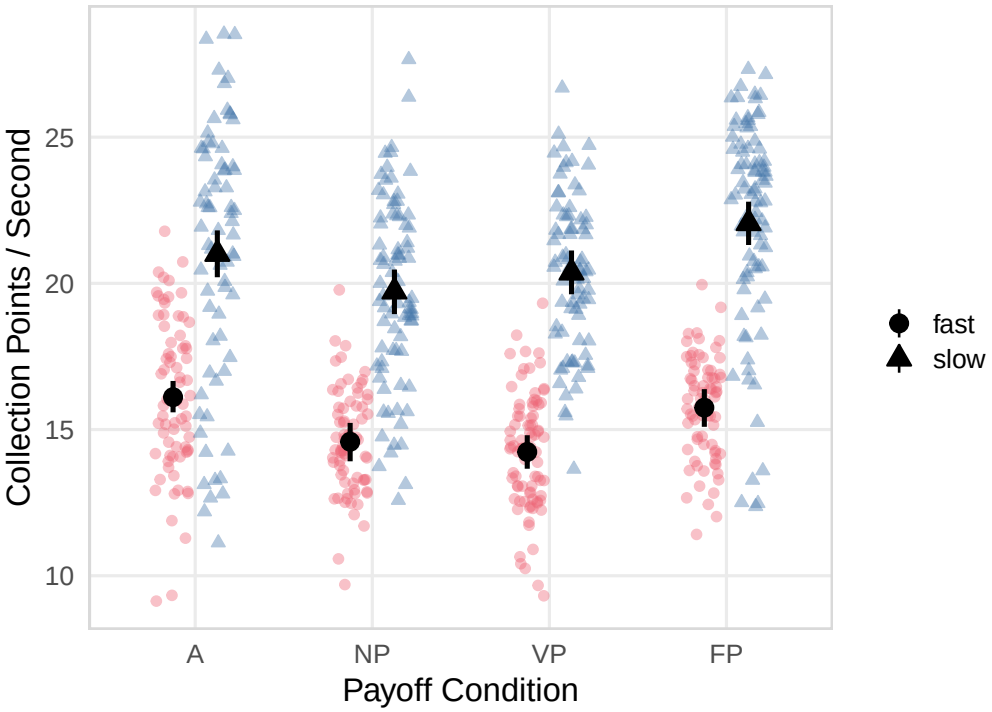

Figure S5: Tracking Efficiency. Mean tracking efficiency (i.e., average number of points earned per second while on the resource) per treatment, shown for each payoff condition (A: Asocial Condition; NP: No Payoff-Sharing; VP: Voluntary Payoff-Sharing; FP: Full Payoff-Sharing) and resource speed (slow vs. fast). Each dot represents an individual participant. Larger black dots and error bars show posterior means and 90% HPDIs.

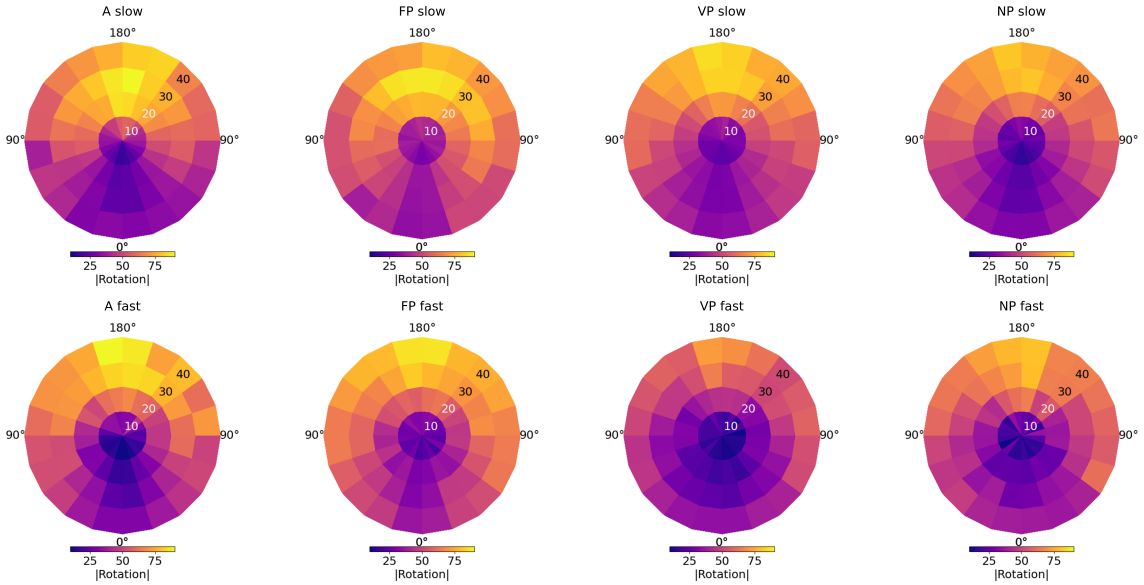

Figure S6: Participants' average rotation magnitude for different positions on the resource, shown for each payoff condition (A: Asocial Condition; NP: No Payoff-Sharing; VP: Voluntary Payoff-Sharing; FP: Full Payoff-Sharing) and resource speed (slow vs. fast).

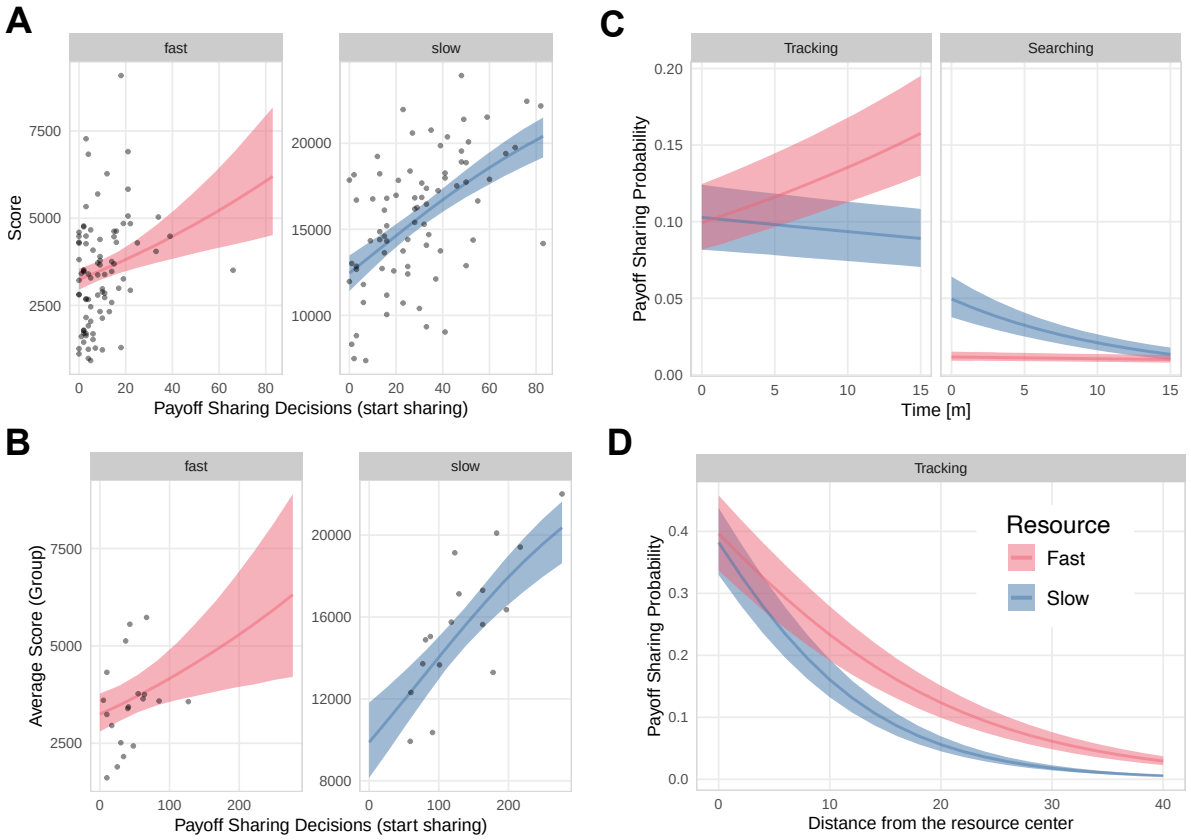

Figure S7: Voluntary Payoff-Sharing Condition. **A** Relationship between the number of individual payoff sharing decisions and final individual score; Each black dot represents an individual participant. **B** Relationship between the total number of sharing decisions within a group and the average group score; Each black dot represents a group. **C** Probability of sharing payoff information at each one-second time step, shown separately for searching and tracking states over the course of the experiment (x-axis). **D** Probability of sharing payoff information at each one-second time step, relative to the distance to the resource center (x-axis). The lines show the posterior predictive mean, and the shade areas the 90% HPDIs.

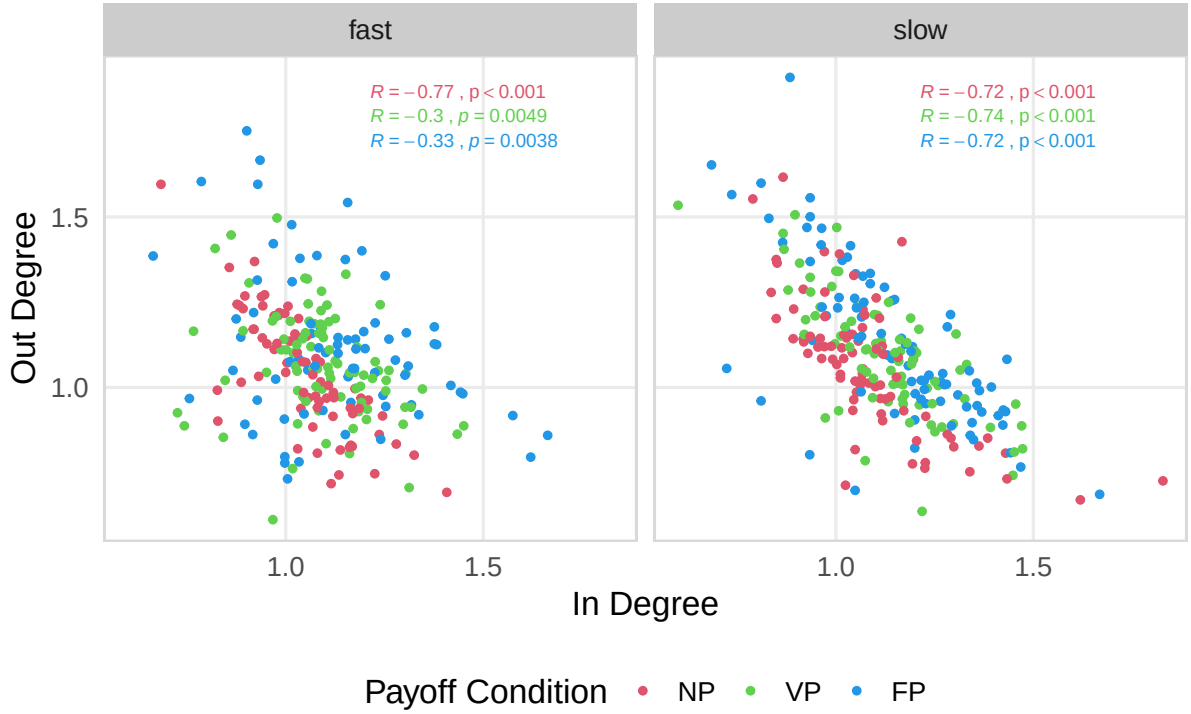

Figure S8: Relationship between In-Degree and Out-Degree for each Payoff Condition. Scatter plots show the mean in-degree and out-degree per participant, colored by payoff condition. NP: No Payoff-Sharing; VP: Voluntary Payoff-Sharing; FP: Full Payoff-Sharing. Separate panels correspond to different resource speed conditions. Pearson's correlation coefficient (r) and p-value are shown in each panel. Across all conditions, in-degree and out-degree were negatively correlated (Pearson's $r = -0.55$, 95% CI $[-0.61, -0.48]$, $p < 0.001$). Each dot represents one participant.

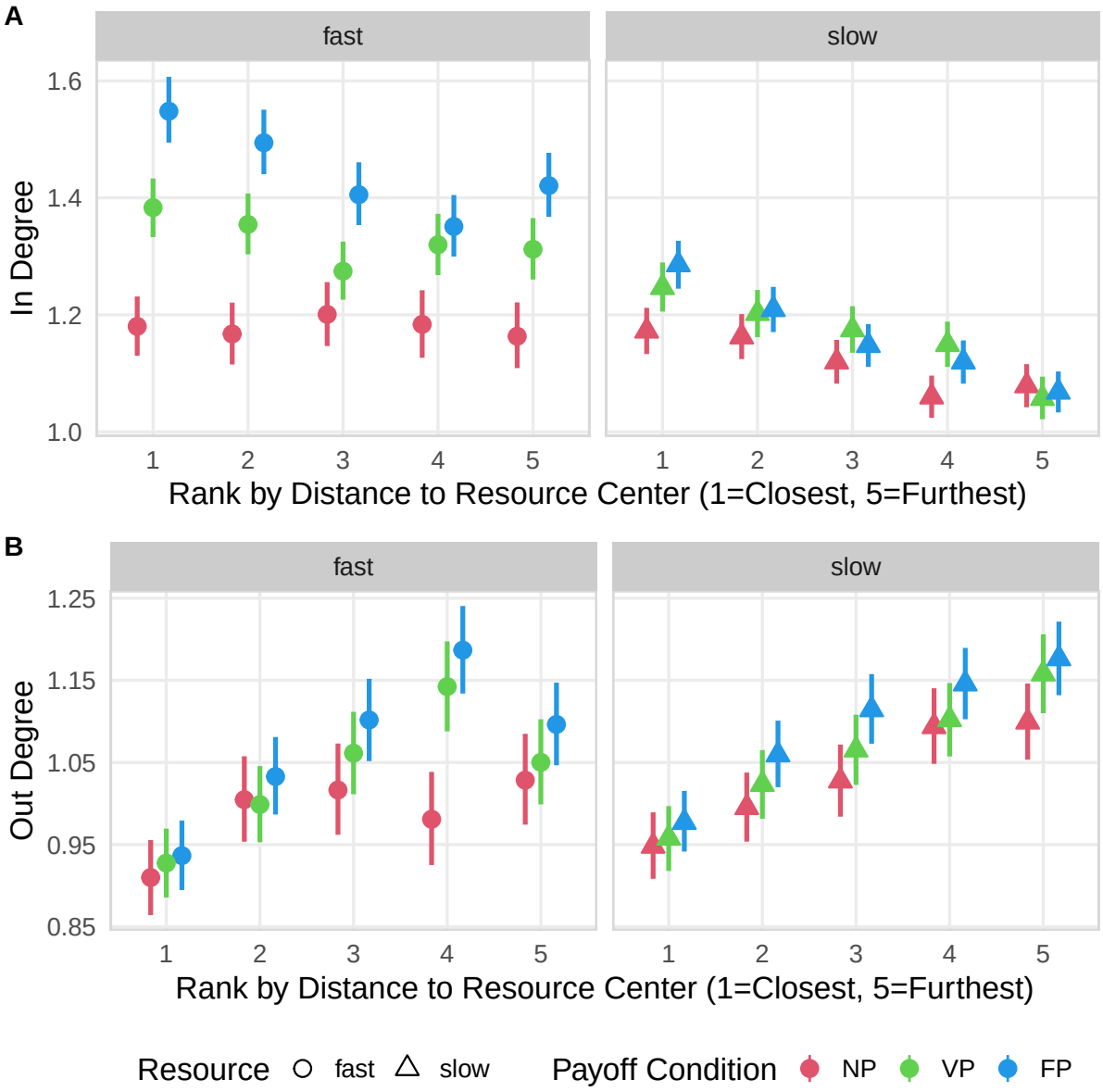

Figure S9: Participant's Distance Rank Relationship to Degree. Average in-degree (**A**) and out-degree (**B**) as a function of each participant's distance rank from the resource center within the group while tracking the resource (i.e., within detection range). Distance rank is assigned per group (1 = closest to resource center, 5 = furthest). Results are shown by payoff sharing condition (color NP: No Payoff-Sharing; VP: Voluntary Payoff-Sharing; FP: Full Payoff-Sharing) and by resource speed (columns). Dots and error bars show posterior means and 90% HPDIs.

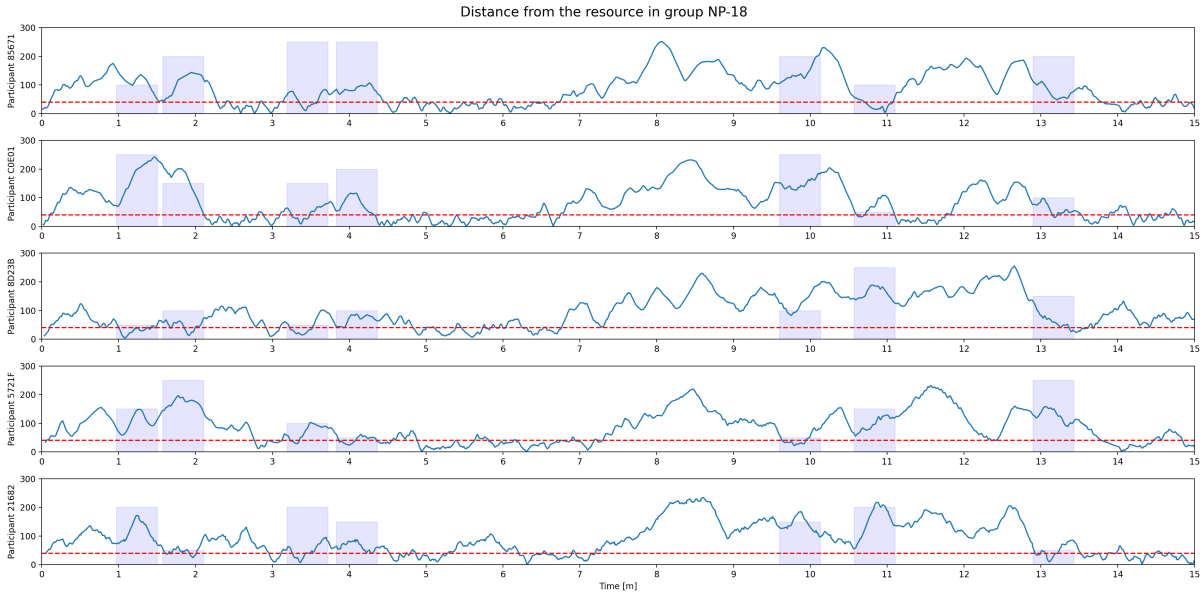

Figure S10: Illustration of resource discovery events. The solid line shows the time series of the distance from the resource for each participant, the dashed line shows the resource detection threshold. Transparent rectangles highlight the resource discovery events. The height of the rectangle indicates the order in which participants crossed the resource discovery area.

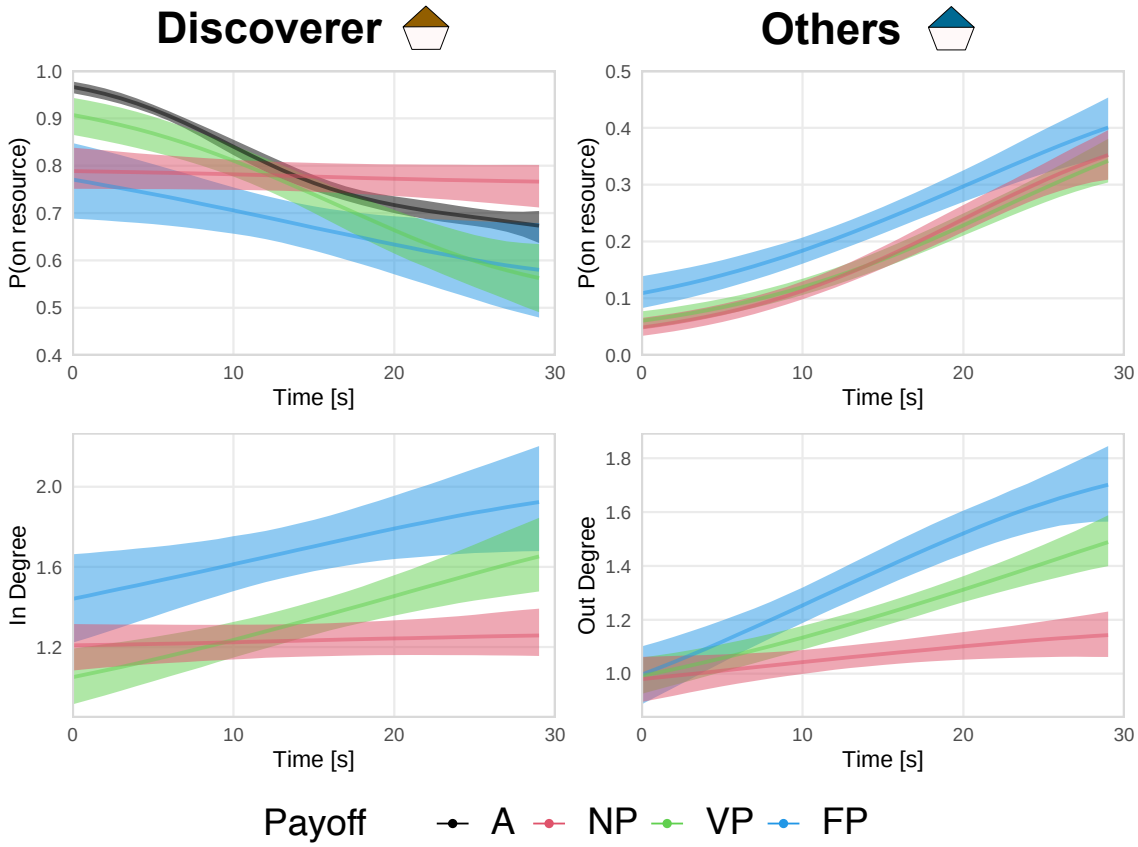

Figure S11: Resource discovery events (slow resource condition). top-left: Probability of remaining on the resource of the first discoverer. **top-right**: Average probability of other players in the group arriving at and staying on the resource. **bottom-left**: Average in-degree of the first player. **bottom-right**: Average out-degree of the other players. A: Asocial Condition; NP: No Payoff-Sharing; VP: Voluntary Payoff-Sharing; FP: Full Payoff-Sharing. Dark lines show posterior means of a Bayesian Gaussian process regression; shades represent 90% HPDIs.

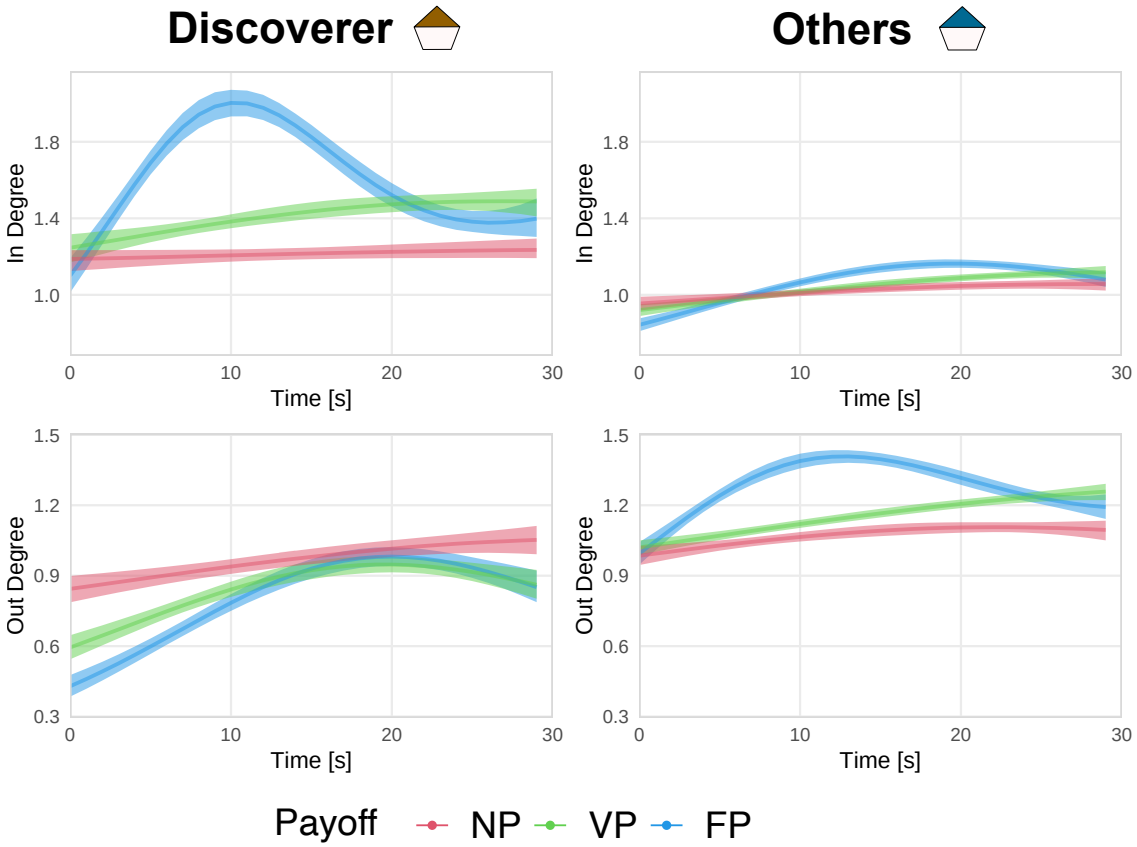

Figure S12: Resource discovery events (fast resource condition; in-/out-degree full). top-left: Average in-degree of the first player. **top-right**: Average in-degree of the other players. **bottom-left**: Average out-degree of the first player. **bottom-right**: Average out-degree of the other players. NP: No Payoff-Sharing; VP: Voluntary Payoff-Sharing; FP: Full Payoff-Sharing. Dark lines show posterior means of a Bayesian Gaussian process regression; shades represent 90% HPDIs.

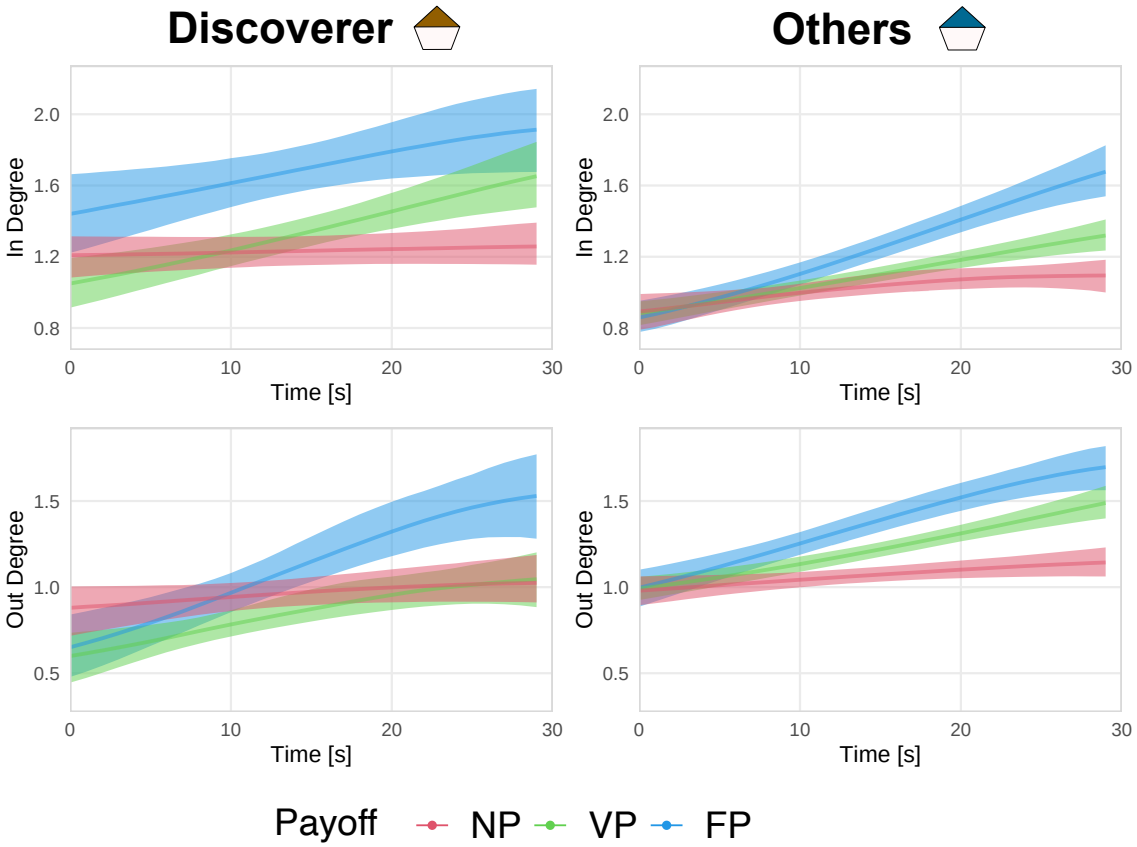

Figure S13: Resource discovery events (slow resource condition; in-/out-degree full). top-left: Average in-degree of the first player. **top-right**: Average in-degree of the other players. **bottom-left**: Average out-degree of the first player. **bottom-right**: Average out-degree of the other players. NP: No Payoff-Sharing; VP: Voluntary Payoff-Sharing; FP: Full Payoff-Sharing. Dark lines show posterior means of a Bayesian Gaussian process regression; shades represent 90% HPDIs.

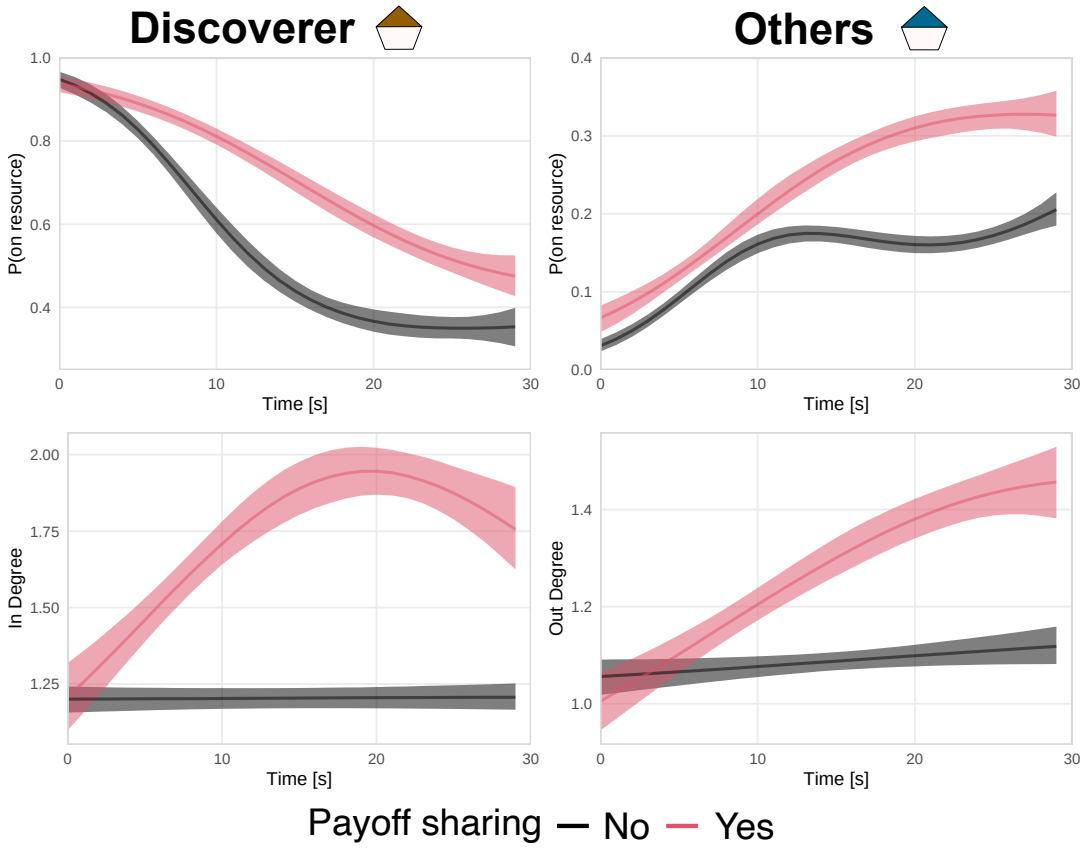

Figure S14: Resource discovery events in VP condition (fast resource condition). top: Schematic of a resource discovery event. **middle-left**: Probability of remaining on the resource of the first discoverer. **middle-right**: Average probability of other players in the group arriving at and staying on the resource. **bottom-left**: Average in-degree of the first player. **bottom-right**: Average out-degree of the other players. The color indicates whether the "discoverer" shared the payoff information for at least two seconds at any point after the event began. Dark lines show posterior means of a Bayesian Gaussian process regression; shades represent 90% HPDIs.

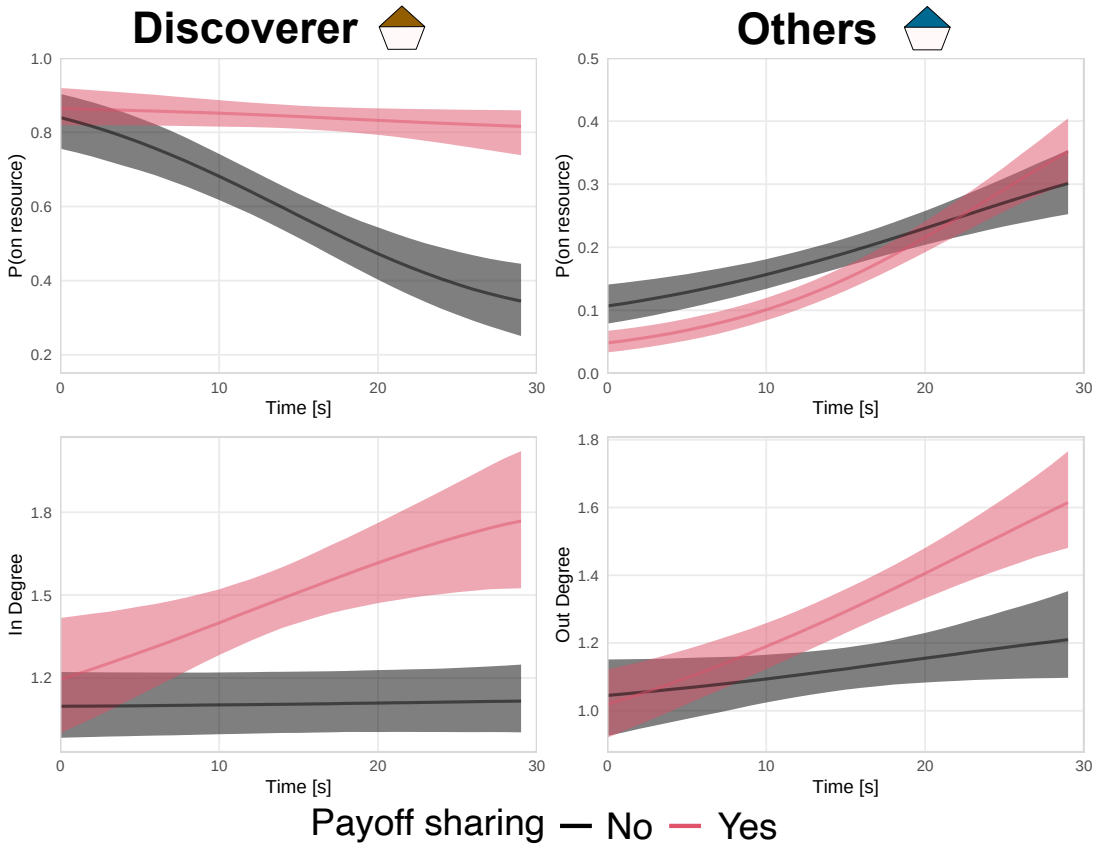

Figure S15: Resource discovery events in VP payoff sharing condition (slow resource condition). top: Schematic of a resource discovery event. **middle-left**: Probability of remaining on the resource of the first discoverer. **middle-right**: Average probability of other players in the group arriving at and staying on the resource. **bottom-left**: Average in-degree of the first player. **bottom-right**: Average out-degree of the other players. The color indicates whether the "discoverer" shared the payoff information for at least two seconds at any point after the event began. Dark lines show posterior means of a Bayesian Gaussian process regression; shades represent 90% HPDIs.

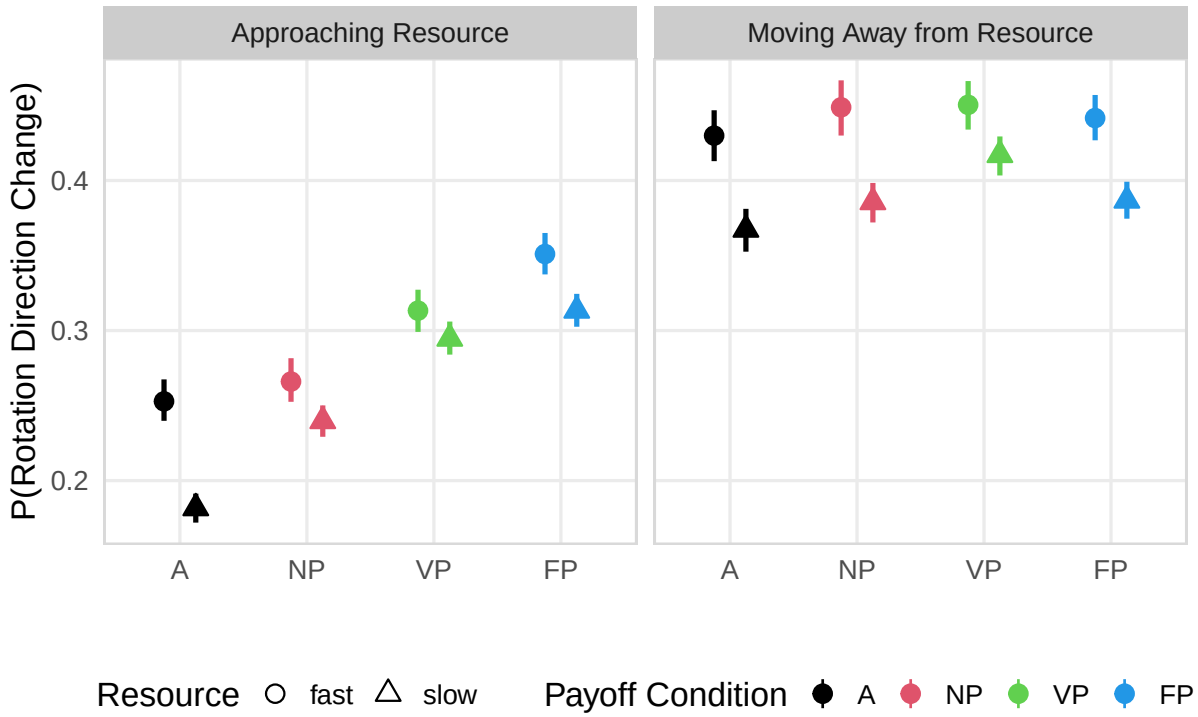

Figure S16: The probability of a rotation direction change as a response to a detector change. The columns show the state of the private information (detector change): the focal agent is approaching (**left panel**) or moving away from the resource center (**right panel**). Color (and the x-axis) denotes the payoff condition (NP: No Payoff-Sharing; VP: Voluntary Payoff-Sharing; FP: Full Payoff-Sharing), and point shape distinguishes the resource speed (slow vs. fast). Dots and error bars show posterior means and 90% HPDIs.

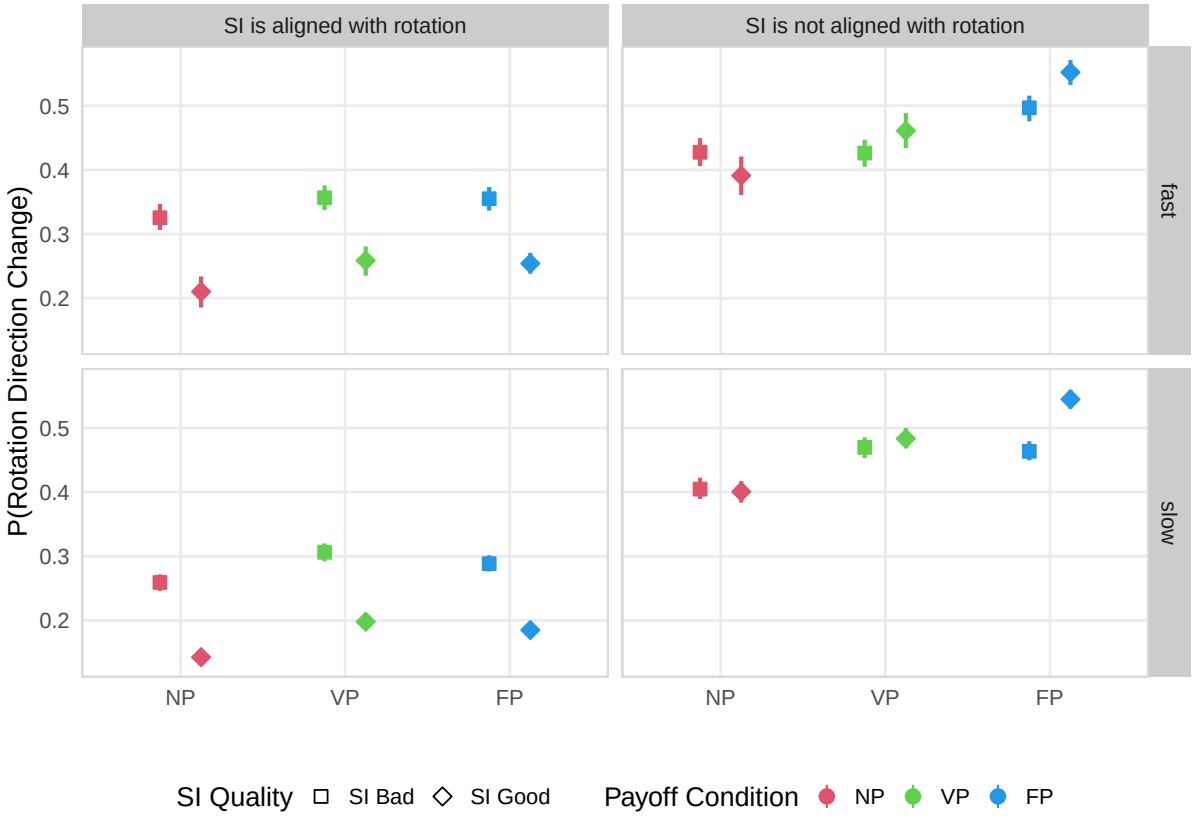

Figure S17: The probability of a change in rotation direction in response to social information (SI) alignment and quality. The columns show the social information state: social information alignment at $t-1$ is aligned (**left panel**) or misaligned (**right panel**) with the preceding rotation direction. The rows indicate resource speed (slow vs. fast). Color (and the x-axis) denotes the payoff condition (NP: No Payoff-Sharing; VP: Voluntary Payoff-Sharing; FP: Full Payoff-Sharing), and point shape indicates social information quality (high=Good vs. low=Bad). Dots and error bars show posterior means and 90% HPDIs.

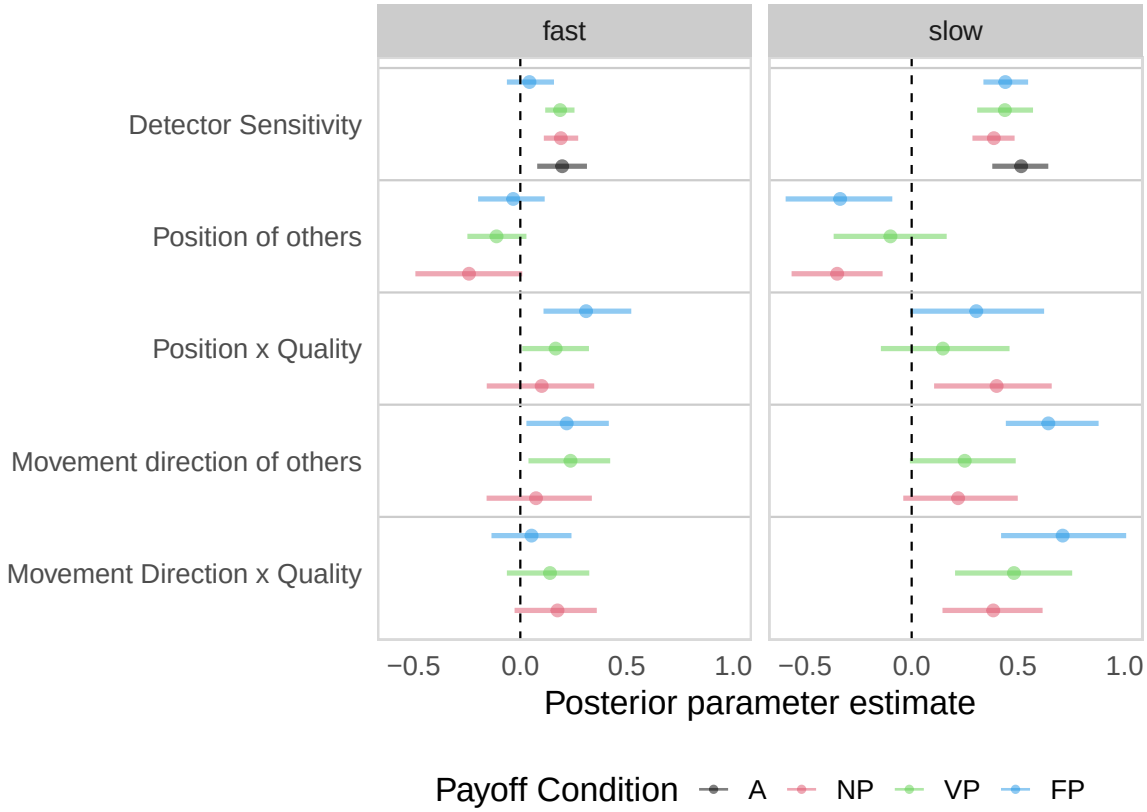

Figure S18: Posterior estimates of the relationship between individual decision weights and tracking efficiency. Individual decision weights are computed in the rotation magnitude model of tracking. Separate models were fit for each feature type (y-axis) and included interactions between payoff sharing condition (color) and resource speed (column). A: Alone Condition; NP: No Payoff-Sharing; VP: Voluntary Payoff-Sharing; FP: Full Payoff-Sharing. Dots and error bars show posterior means and 90% HPDIs.

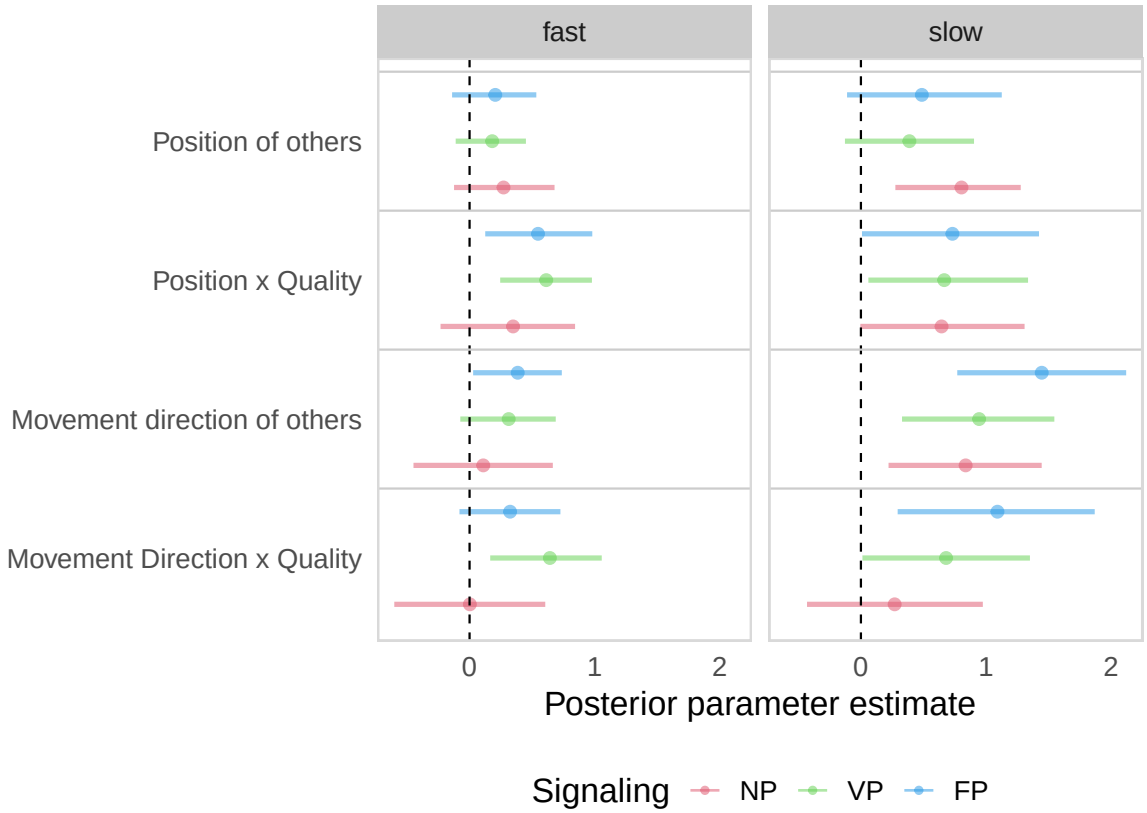

Figure S19: Posterior estimates of the relationship between individual decision weights and tracking time. Individual decision weights are computed in the rotation magnitude model of searching. Separate models were fit for each feature type (y-axis) and included interactions between payoff sharing condition (color) and resource speed (column). A: Alone Condition; NP: No Payoff-Sharing; VP: Voluntary Payoff-Sharing; FP: Full Payoff-Sharing. Dots and error bars show posterior means and 90% HPDIs.

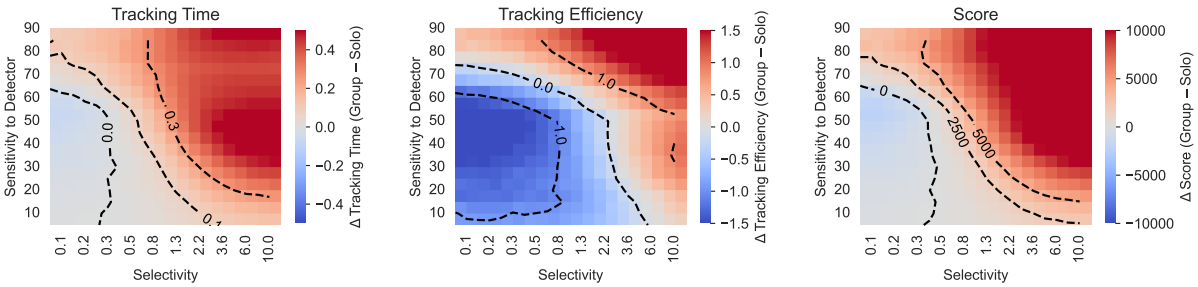

Figure S20: Effect of selectivity in the use of social information: agent-based simulation. Agent-based model parameter sweep for detector sensitivity (x-axis) and social information selectivity (y-axis). The value in each cell is calculated as the difference between average group and solitary performance. Higher detector sensitivity corresponds to a rotation that is closer to the optimal rotation for a given change in detector value. Greater selectivity corresponds to a steeper social information curve (see Fig. 5A). Each panel shows the difference in key performance measures between average group performance and solitary performance: tracking time (**left**), tracking efficiency (**middle**), and total score (**right**).

S2 Supplementary Tables

Table S1: Participant Distribution Across Experimental Conditions

Payoff	Resource	Participants	Groups	Groups of 5	Groups of 4
A	Fast	73	73	–	–
A	Slow	71	71	–	–
NP	Fast	72	15	12	3
NP	Slow	80	17	12	5
VP	Fast	86	19	10	9
VP	Slow	79	17	11	6
FP	Fast	74	17	6	11
FP	Slow	86	18	14	4

Note: The table shows participant and group counts by payoff sharing and resource speed conditions. "Groups of 5" and "Groups of 4" indicate the number of groups that had exactly 5 or 4 valid participants, respectively. A: Asocial Condition, NP: No Payoff-Sharing; VP: Voluntary Payoff-Sharing; FP: Full Payoff-Sharing..

Table S2: Posterior Estimates Collected Points

Resource Speed	Payoff Condition	Contrast	Mean	90% HPDI
.	.	slow - fast	**10720.57**	**[9832.10, 11606.53]**
.	A	slow - fast	**8449.69**	**[7053.20, 9863.92]**
.	FP	slow - fast	**11975.64**	**[10337.88, 13668.39]**
.	NP	slow - fast	**10571.08**	**[8863.52, 12276.49]**
.	VP	slow - fast	**11885.87**	**[10325.95, 13444.91]**
fast				
fast	.	FP - A	**1710.26**	**[572.81, 2803.50]**
fast	.	FP - NP	**2544.92**	**[1364.50, 3718.67]**
fast	.	FP - VP	**2008.92**	**[843.34, 3194.27]**
fast	.	NP - A	**-834.66**	**[-1654.19, -35.59]**
fast	.	VP - A	-298.66	[-1169.61, 537.86]
fast	.	VP - NP	536.00	[-385.41, 1471.24]
slow				
slow	.	FP - A	**5236.22**	**[3373.83, 7129.94]**
slow	.	FP - NP	**3949.48**	**[1876.26, 6081.79]**
slow	.	FP - VP	**2098.69**	**[84.14, 4069.94]**
slow	.	NP - A	1286.73	[-790.97, 3366.14]
slow	.	VP - A	**3137.53**	**[1126.32, 5079.08]**
slow	.	VP - NP	1850.79	[-316.14, 4021.80]

Note: Contrasts where the 90% HPDI does not include zero are highlighted in bold. '90% HPDI' refers to the 90% highest posterior density interval. 'Mean' is the mean of the posterior distribution for each contrast.

Table S3: Posterior Estimates Collected Points Precision

Resource Speed	Payoff Condition	Contrast	Mean	90% HPDI
.	.	slow - fast	**0.42**	**[0.38, 0.45]**
.	A	slow - fast	**0.33**	**[0.28, 0.38]**
.	FP	slow - fast	**0.47**	**[0.40, 0.53]**
.	NP	slow - fast	**0.41**	**[0.35, 0.48]**
.	VP	slow - fast	**0.46**	**[0.40, 0.52]**
fast				
fast	.	FP - A	**0.07**	**[0.02, 0.11]**
fast	.	VP - A	-0.01	[-0.05, 0.02]
fast	.	NP - A	-0.03	[-0.06, -0.00]
fast	.	FP - NP	**0.10**	**[0.05, 0.15]**
fast	.	FP - VP	**0.08**	**[0.03, 0.12]**
fast	.	VP - NP	0.02	[-0.02, 0.06]
slow				
slow	.	FP - A	**0.20**	**[0.13, 0.28]**
slow	.	VP - A	**0.12**	**[0.04, 0.20]**
slow	.	NP - A	0.05	[-0.03, 0.13]
slow	.	FP - NP	**0.15**	**[0.07, 0.24]**
slow	.	FP - VP	0.08	[0.00, 0.16]
slow	.	VP - NP	0.07	[-0.01, 0.16]

Note: Contrasts where the 90% HPDI does not include zero are highlighted in bold. The column labeled 'Mean' gives the posterior mean of the difference in the Beta precision parameter (ϕ) between conditions, on the response scale (not log-transformed). The '90% HPDI' shows the 90% highest posterior density interval for each contrast. Higher values of ϕ indicate greater precision (i.e., less variability) in the outcome distribution.

Table S4: Posterior Estimates Tracking Time (minutes)

Resource Speed	Payoff Condition	Contrast	Mean	90% HPDI
.	.	slow - fast	**7.44**	**[6.89, 8.00]**
.	A	slow - fast	**5.96**	**[5.13, 6.80]**
.	FP	slow - fast	**7.43**	**[6.40, 8.44]**
.	NP	slow - fast	**7.97**	**[6.86, 9.03]**
.	VP	slow - fast	**8.41**	**[7.47, 9.39]**
fast				
fast	.	FP - A	**2.00**	**[0.96, 3.04]**
fast	.	FP - NP	**2.33**	**[1.07, 3.55]**
fast	.	FP - VP	**1.76**	**[0.56, 3.01]**
fast	.	NP - A	-0.34	[-1.22, 0.56]
fast	.	VP - A	0.23	[-0.66, 1.13]
fast	.	VP - NP	0.57	[-0.52, 1.68]
slow				
slow	.	FP - A	**3.47**	**[2.63, 4.32]**
slow	.	FP - NP	**1.80**	**[0.84, 2.74]**
slow	.	FP - VP	**0.78**	**[0.01, 1.56]**
slow	.	NP - A	**1.67**	**[0.56, 2.71]**
slow	.	VP - A	**2.68**	**[1.75, 3.63]**
slow	.	VP - NP	1.01	[-0.03, 2.05]

Note: Contrasts where the 90% HPDI does not include zero are highlighted in bold. '90% HPDI' refers to the 90% highest posterior density interval. 'Mean' is the mean of the posterior distribution for each contrast.

Table S5: Posterior Estimates Tracking Efficiency (points/second)

Resource Speed	Payoff Condition	Contrast	Mean	90% HPDI
.	.	slow - fast	**5.62**	**[5.13, 6.11]**
.	A	slow - fast	**4.90**	**[3.95, 5.85]**
.	FP	slow - fast	**6.31**	**[5.34, 7.29]**
.	NP	slow - fast	**5.14**	**[4.12, 6.13]**
.	VP	slow - fast	**6.14**	**[5.19, 7.08]**
fast				
fast	.	FP - A	-0.36	[-1.21, 0.46]
fast	.	FP - NP	**1.17**	**[0.25, 2.09]**
fast	.	FP - VP	**1.52**	**[0.64, 2.37]**
fast	.	NP - A	**-1.53**	**[-2.37, -0.68]**
fast	.	VP - A	**-1.88**	**[-2.64, -1.09]**
fast	.	VP - NP	-0.35	[-1.23, 0.52]
slow				
slow	.	FP - A	1.05	[-0.02, 2.16]
slow	.	FP - NP	**2.34**	**[1.25, 3.38]**
slow	.	FP - VP	**1.69**	**[0.63, 2.73]**
slow	.	NP - A	**-1.29**	**[-2.38, -0.16]**
slow	.	VP - A	-0.64	[-1.73, 0.46]
slow	.	VP - NP	0.65	[-0.42, 1.72]

Note: Contrasts where the 90% HPDI does not include zero are highlighted in bold. '90% HPDI' refers to the 90% highest posterior density interval. 'Mean' is the mean of the posterior distribution for each contrast.

Table S6: Posterior Estimates In Degree

Resource Speed	Payoff Condition	Contrast	Mean	90% HPDI
.	FP	slow - fast	0.02	[-0.03, 0.06]
.	NP	slow - fast	0.04	[-0.01, 0.08]
.	VP	slow - fast	0.03	[-0.01, 0.07]
fast				
fast	.	FP - NP	**0.08**	**[0.03, 0.12]**
fast	.	FP - VP	0.03	[-0.02, 0.07]
fast	.	VP - NP	**0.05**	**[0.01, 0.09]**
slow				
slow	.	FP - NP	**0.06**	**[0.01, 0.10]**
slow	.	FP - VP	0.01	[-0.03, 0.06]
slow	.	VP - NP	0.04	[0.00, 0.09]

Note: Contrasts where the 90% HPDI does not include zero are highlighted in bold. '90% HPDI' refers to the 90% highest posterior density interval. 'Mean' is the mean of the posterior distribution for each contrast.

Table S7: Posterior Estimates Out Degree

Resource Speed	Payoff Condition	Contrast	Mean	90% HPDI
.	FP	slow - fast	0.01	[-0.04, 0.06]
.	NP	slow - fast	0.02	[-0.03, 0.07]
.	VP	slow - fast	0.02	[-0.03, 0.07]
fast				
fast	.	FP - NP	**0.07**	**[0.02, 0.12]**
fast	.	FP - VP	0.04	[-0.01, 0.09]
fast	.	VP - NP	0.03	[-0.02, 0.08]
slow				
slow	.	FP - NP	**0.06**	**[0.01, 0.11]**
slow	.	FP - VP	0.03	[-0.02, 0.08]
slow	.	VP - NP	0.03	[-0.02, 0.08]

Note: Contrasts where the 90% HPDI does not include zero are highlighted in bold. '90% HPDI' refers to the 90% highest posterior density interval. 'Mean' is the mean of the posterior distribution for each contrast.

Table S8: Posterior Estimates Adaptive Connectivity: Probability to Follow Adaptive Social Information.

Resource	Payoff	State	Contrast	Mean	90% HPDI
.	FP	searching	slow - fast	**0.03**	**[0.01, 0.05]**
.	NP	searching	slow - fast	**0.11**	**[0.09, 0.14]**
.	VP	searching	slow - fast	**0.08**	**[0.05, 0.10]**
.	FP	tracking	slow - fast	**-0.02**	**[-0.04, -0.01]**
.	NP	tracking	slow - fast	**0.07**	**[0.05, 0.09]**
.	VP	tracking	slow - fast	**0.05**	**[0.03, 0.07]**
fast					
fast	FP	.	searching - tracking	**-0.02**	**[-0.03, -0.01]**
fast	NP	.	searching - tracking	**-0.08**	**[-0.10, -0.07]**
fast	VP	.	searching - tracking	**-0.05**	**[-0.06, -0.04]**
fast	.	searching	FP - NP	**0.20**	**[0.18, 0.23]**
fast	.	searching	FP - VP	**0.13**	**[0.11, 0.15]**
fast	.	searching	VP - NP	**0.08**	**[0.06, 0.10]**
fast	.	tracking	FP - NP	**0.14**	**[0.12, 0.16]**
fast	.	tracking	FP - VP	**0.10**	**[0.08, 0.12]**
fast	.	tracking	VP - NP	**0.04**	**[0.02, 0.07]**
slow					
slow	FP	.	searching - tracking	**0.03**	**[0.02, 0.05]**
slow	NP	.	searching - tracking	**-0.04**	**[-0.06, -0.03]**
slow	VP	.	searching - tracking	**-0.03**	**[-0.04, -0.01]**
slow	.	searching	FP - NP	**0.12**	**[0.10, 0.15]**
slow	.	searching	FP - VP	**0.08**	**[0.06, 0.11]**
slow	.	searching	VP - NP	**0.04**	**[0.02, 0.06]**
slow	.	tracking	FP - NP	**0.05**	**[0.03, 0.06]**
slow	.	tracking	FP - VP	**0.02**	**[0.01, 0.04]**
slow	.	tracking	VP - NP	**0.02**	**[0.01, 0.04]**

Note: All contrasts are calculated conditional on **adaptive social information being available**. Contrasts where the 90% HPDI does not include zero are highlighted in bold. '90% HPDI' refers to the 90% highest posterior density interval. 'Mean' is the mean of the posterior distribution for each contrast.

Table S9: Number of Resource Discovery Events per Condition

Payoff Condition	Resource Speed	Unique Events
A	Fast	383
NP	Fast	126
VP	Fast	173
FP	Fast	147
A	Slow	212
NP	Slow	17
VP	Slow	21
FP	Slow	11

Note: The table shows the number of unique resource discovery events by payoff sharing and resource speed conditions. A: Asocial Condition, NP: No Payoff-Sharing; VP: Voluntary Payoff-Sharing; FP: Full Payoff-Sharing.

S3 Data Collection

Data collection was conducted over three periods in 2023: April 11-12, May 3, and November 13-17. On April 11-12, data were collected for the A, NP, and FP conditions (both fast and slow). On May 3, data were collected for the VP condition (both fast and slow). Roughly half of the samples within each condition were collected in these first two periods (n = 329 participants). The remaining half of the samples in all conditions were collected from November 13-17. For each experimental condition (e.g., Full Payoff Sharing and slow resource), participants were recruited separately within a given time interval, typically 2 hours. To maximize the number of complete groups, we opened 50 slots simultaneously per experimental condition on Prolific. This number was dictated by the bandwidth capabilities of the game server. Participants could only join newly forming groups before the start of the experiment; once a session had begun, no additional participants could enter. If a participant dropped out during the experiment, this participant was not replaced. For analysis, we only included groups that finished with at least four players (see Table S1 for the number of groups per condition). In total, the data collection consisted of 16 2-hour sessions on Prolific.

S4 Optimal rotation based on private information

Here, we derive a normative model to determine the optimal rotation an agent should make based solely on the change in its distance to a moving resource (δ_t). The derivation consists of two parts. First, a **forward model** calculates how the distance to the resource changes as a function of the agent's movement relative to resource. This answers the question: Given my movement, what distance change should I expect? Second, an **inverse model** uses Bayesian inference to invert this logic, answering the question: Given the distance change I just observed, what is the optimal way to turn?

S4.1 Forward model: calculating distance change

The forward model calculates the rate of change in distance ($\frac{d}{dt}r$) between an agent and a resource, given their speeds and relative orientation. We establish a reference frame that moves with the resource, with the resource's velocity vector, $\vec{v}_p$ (see Fig. S1A). The relevant variables are: The agent's constant speed (v_a); The resource's constant speed (v_p); The agent's heading, relative to the resource's direction of motion (ϕ_a); The angle of the agent's position, relative to the resource's direction of motion (ξ).

The rate of change in distance is the projection of the relative velocity vector ($\vec{v}_a - \vec{v}_p$) onto the unit vector ($\hat{u}_r$) that points from the resource to the agent.

$$\frac{d}{dt}r = (\vec{v}_a - \vec{v}_p) \cdot \hat{u}_r \tag{S1}$$

In the resource frame of reference, the vectors are: resource velocity: $\vec{v}_p = v_p \begin{bmatrix} \cos(0) \\ \sin(0) \end{bmatrix}$; agent velocity: $\vec{v}_a = v_a \begin{bmatrix} \cos(\phi_a) \\ \sin(\phi_a) \end{bmatrix}$; unit vector to agent: $\hat{u}_r = \begin{bmatrix} \cos(\xi) \\ \sin(\xi) \end{bmatrix}$. Performing the dot product:

$$
\begin{aligned}
\frac{d}{dt}r &= \begin{bmatrix} v_a\cos(\phi_a) - v_p\cos(0) \\ v_a\sin(\phi_a) - v_p\sin(0) \end{bmatrix} \cdot \begin{bmatrix} \cos(\xi) \\ \sin(\xi) \end{bmatrix} \\
&= \begin{bmatrix} v_a\cos(\phi_a) - v_p \\ v_a\sin(\phi_a) \end{bmatrix} \cdot \begin{bmatrix} \cos(\xi) \\ \sin(\xi) \end{bmatrix} \\
&= (v_a\cos(\phi_a) - v_p)\cdot\cos(\xi) + v_a\sin(\phi_a)\cdot\sin(\xi) \\
&= v_a\cdot(\cos(\phi_a)\cdot\cos(\xi) + \sin(\phi_a)\cdot\sin(\xi)) - v_p\cdot\cos(\xi)
\end{aligned}
\tag{S2}
$$

Using the trigonometric identity for the cosine of a difference (i.e., $\cos(\alpha-\beta) = \cos(\alpha)\cos(\beta) + \sin(\alpha)\sin(\beta)$) we arrive at the final expression for the forward model (see Fig. S1B):

$$
\frac{d}{dt}r = v_a\cos(\phi_a - \xi) - v_p\cos(\xi) \tag{S3}
$$

S4.2 Optimal rotation

To find the optimal rotation, ψ, an agent must choose the turn that will most rapidly decrease its distance to the resource. This corresponds to minimizing the future rate of distance change. After a rotation ψ, the agent's new heading will be $\phi_a' = \phi_a + \psi$. We therefore minimize the following function (forward model) with respect to ψ:

$$
f(\psi) = v_a\cos(\phi_a + \psi - \xi) - v_p\cos(\xi) \tag{S4}
$$

The first derivative with respect to ψ is:

$$
\frac{df}{d\psi} = -v_a\sin(\phi_a + \psi - \xi) \tag{S5}
$$

Setting the first derivative to zero finds the extrema:

$$
-v_a\sin(\phi_a + \psi - \xi) = 0 \Rightarrow \psi = \pm\pi + \xi - \phi_a \vee \psi = \xi - \phi_a \tag{S6}
$$

The second derivative with respect to ψ is:

$$
\frac{df^2}{d\psi^2} = -v_a\cos(\phi_a + \psi - \xi) \tag{S7}
$$

The second derivative of the function should be positive (indicating a minimum):

$$
\begin{aligned}
-v_a\cos(\phi_a + \psi - \xi) &> 0 \\
\cos(\phi_a + \psi - \xi) &< 0 \\
-\frac{\pi}{2} > \phi_a + \psi - \xi \vee \phi_a + \psi - \xi &> \frac{\pi}{2} \\
-\frac{\pi}{2} + \xi - \phi_a > \psi \vee \psi &> \frac{\pi}{2} + \xi - \phi_a
\end{aligned}
\tag{S8}
$$

Thus, the optimal rotation is (see Fig. S1C):

$$
\psi_{\text{opt}} = \pm\pi + \xi - \phi_a \tag{S9}
$$

Note that based on the distance change δ alone there are **two** possible optimal solutions.

S4.3 Inference model: inferring rotation from distance change

In the hidden resource tracking task, an agent doesn't know the true angles ξ and ϕ_a; it only observes the resulting distance change, $\delta_t \approx \frac{d}{dt}r$. The inverse model uses this observation to infer a probability distribution over possible optimal rotations. Using Bayes' rule, we seek the posterior probability of a rotation ψ given an observed distance change δ: $P(\psi|\delta)$. We can find this by marginalizing over the unknown (latent) angles ξ and ϕ_a:

$$P(\psi|\delta) = \int_{-\pi}^{+\pi} \int_{-\pi}^{+\pi} p(\psi|\delta, \xi, \phi_a) \cdot p(\xi, \phi_a)\, \mathrm{d}\xi\, \mathrm{d}\phi_a \tag{S10}$$

We make three simplifying assumptions. First, we assume the optimal rotation is determined by the latent angles. Once ξ and ϕ_a are known, the optimal rotation ψ_{opt} is fixed (see Eq. S9). Second, we assume conditional independence of ψ and δ given ξ and ϕ_a, and therefore express $P(\psi|\xi, \phi_a, \delta)$ as following:

$$P(\psi|\xi, \phi_a, \delta) \propto P(\psi|\xi, \phi_a) \cdot P(\delta|\xi, \phi_a) \cdot P(\xi, \phi_a) \tag{S11}$$

Third, we assume a uniform prior over angles, meaning the agent has no prior knowledge of its relative orientation, so $p(\xi, \phi_a)$ is a uniform distribution. Under these assumptions, Bayes' rule simplifies the posterior to:

$$P(\psi|\delta) \propto \int_{-\pi}^{+\pi} \int_{-\pi}^{+\pi} p(\psi|\xi, \phi_a) \cdot p(\delta|\xi, \phi_a)\, \mathrm{d}\xi\, \mathrm{d}\phi_a \tag{S12}$$

Here, $p(\delta|\xi, \phi_a)$ is the likelihood of observing δ given a specific orientation, which is derived from the forward model. $p(\psi|\xi, \phi_a)$ is the policy that executes the optimal rotation ψ_{opt} for a given orientation and could be substituted with the expression from Eq. S9. To compute this numerically, we approximate the integral by summing over a discrete grid of $N \times N$ possible values for ξ and ϕ_a:

$$P(\psi|\delta) \approx \sum_{i=1}^{N} \sum_{j=1}^{N} p(\psi|\xi_i, \phi_{a,j}) \cdot p(\delta|\xi_i, \phi_{a,j})\, \Delta\xi\, \Delta\phi_a \tag{S13}$$

where $\Delta\xi$ and $\Delta\phi_a$ are the steps in the discretization of the domain $[-\pi, \pi] \times [-\pi, \pi]$. For an illustration of the inference model, see Fig. S1D-F and Fig. S2 for the inference model for the different resource speeds (v_p).

S5 Voluntary Payoff-Sharing Condition

In the Voluntary Payoff-Sharing condition, participants could decide whether to share their current payoff with group members. Sharing was initiated by pressing the space bar, which activated a visible payoff beam above the avatar, similar to the Full Payoff-Sharing condition. Once activated, sharing continued until the space bar was pressed again, with each sharing episode lasting at least one second, even if participants immediately stopped. Sharing came at a small cost of 1 point per second.

Out of 165 participants, only 12 (7.3%) never shared payoff information (2 in the slow-resource condition, 10 in the fast-resource condition). On average, participants initiated payoff sharing 6.58 times [5.60, 7.59] in the fast-resource condition and 20.88 times [17.79, 23.96] in the slow-resource condition (posterior estimates from a Bayesian Poisson regression). These sharing episodes corresponded to average sharing durations of 1.64 minutes [1.37, 1.91] in the fast condition and 2.24 minutes [1.90, 2.55] in the slow condition (posterior estimates from a Bayesian Beta regression), with the individual

sharing for the longest period reaching 13.33 minutes.

The frequency of sharing decisions was positively associated with individual performance (Fig. S7A), and the total number of sharing decisions within a group was associated with the group's average score (Fig. S7B). Both associations were credibly stronger in the slow-resource condition. By contrast, the total time spent sharing was not reliably linked to higher scores at either the individual or group level.

We next examined payoff sharing at a more fine-grained scale by modeling the probability of sharing at one-second time steps. As expected, participants were more likely to share when tracking the resource compared to searching for it, in both the fast (0.12 [0.09, 0.14]) and slow (0.07 [0.06, 0.08]) condition (Fig. S7C). Over time, sharing became more common in the fast condition when participants were tracking (0.06 [0.04, 0.08]). Interestingly, in the slow condition participants shared payoff information more selectively compared to the fast condition, sharing less during tracking when they were far from the resource center, but equally when very close to it (Fig. S7D).

S6 Rotation Direction Analysis

This supplementary analysis complements the rotation–magnitude results presented in the main text. Here we ask when participants reverse their rotation direction (i) in response to changes in detector values (Fig. S16) and (ii) as a function of the spatial configuration and quality of social information (Fig. S17).

Across payoff conditions, participants changed rotation direction more often in the fast-resource condition, consistent with adaptation to higher environmental volatility. Beyond this general effect, rotation direction changes followed a simple heuristic: Keep turning in the same direction when moving toward the resource center; reverse when moving away. As in the rotation–magnitude analysis, groups were less responsive to the detector than singletons, especially while approaching the resource (Fig. S16 left).

Social information was classified as *aligned with rotation* when it appeared in the FOV sector toward which the participant had just rotated. Figure S17 shows how the probability of a rotation direction change at time t depends on social information alignment at $t-1$. We also distinguished between two levels of social information quality, depending on whether the observed peer was closer to (good) or farther from (bad) the resource center than the focal individual.

In all group conditions, alignment with social information lowered the chance of a rotation direction change. However, when the social information was of low quality, the probability of a rotation direction change was substantially higher than when the participant was aligned with high-quality social information. The fact that participants were sensitive to the quality of social information when it was aligned with a rotation direction change in all payoff conditions might indicate that it was simple for them to evaluate the quality of social information in this case.

When social information was not aligned with the rotation direction, rotation direction change probability increased overall. However, its interaction with social information quality differed across payoff conditions. NP groups treated high- and low-quality social information similarly, whereas FP groups changed the rotation direction more often when misaligned with high-quality social information (see Fig. S17 right).

Taken together, decisions about rotation direction integrate private cues, the spatial alignment of social cues, and their relative quality. Payoff conditions govern sensitivity to social information quality. These patterns complement the findings reported in the main text.

S7 Rotation Magnitude Model Random Effects Analysis

To assess the relationship between individual decision-making strategies and success, we extracted subject-level random effects (i.e., individual-specific weights) from the multilevel computational model of rotation magnitude. We then used these weights to predict behavioral outcomes. For tracking, we modeled tracking efficiency as a function of each individual's private and social weights. We modeled tracking efficiency separately for each weight using experimental conditions as fixed effects. The results are shown in Fig. S18 and discussed in the Results section of the main text. We repeated this analysis for rotation magnitude model of searching, using tracking time as the outcome. The results are shown in Fig. S19.

S8 Agent-Based Modeling: Interaction Between Private Sensitivity and Social Selectivity

We used the agent-based model presented in the main text to explore how private and social information use interacted in shaping performance. Fig. S20 plots relative (to solitary agents) tracking time (left), tracking efficiency (center) and total score (right) for different degrees of selectivity to social information (on the x-axis) and sensitivity to the detector, i.e., changes in payoffs (on the y-axis). Increasing detector sensitivity allows agents to rotate more optimally, with a theoretical maximum detector sensitivity of 90 degrees. Blue cells corresponds to regions in parameter space where social agents perform worse than solitary agents, red cells correspond to regions where social agents perform better. The results show that the selectivity of social information plays a larger role when social agents are imperfect individual trackers. This is particularly evident in the lower part of Fig. S20 (middle panel), where agents with lower detector sensitivity tend to perform worse than singletons unless they are highly selective in their use of social information. Conversely, in the upper part of the plot - where agents have high detector sensitivity - there is no indication that social agents fall below singleton performance, even at the lowest levels of selectivity. This suggests that when agents are near-perfect individual trackers, less selective use of social information still provides a comparative performance advantage over solitary conditions. They can closely track changes in payoffs, limiting the risks of maladaptive herding and information cascades. In addition, they may benefit more from copying, as others in the group are more likely to make optimal decisions and thus provide adaptive information.